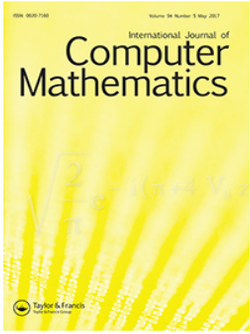

International Journal of Computer Mathematics

ISSN: 0020-7160 (Print) 1029-0265 (Online) Journal homepage: http://www.tandfonline.com/loi/gcom20

Stochastic volatility double-jump-diffusions model: the importance of distribution type of jump amplitude

Youfa Sun, Caiyan Liu & Shimin Guo

To cite this article: Youfa Sun, Caiyan Liu & Shimin Guo (2017) Stochastic volatility double-jump-diffusions model: the importance of distribution type of jump amplitude, International Journal of Computer Mathematics, 94:5, 989-1014, DOI: 10.1080/00207160.2016.1158814

To link to this article: https://doi.org/10.1080/00207160.2016.1158814

Accepted author version posted online: 28 Feb 2016.
Published online: 30 Mar 2016.

INTERNATIONAL JOURNAL OF COMPUTER MATHEMATICS, 2017
VOL. 94, NO. 5, 989–1014
http://dx.doi.org/10.1080/00207160.2016.1158814

Stochastic volatility double-jump-diffusions model: the importance of distribution type of jump amplitude

Youfa Sun [a], Caiyan Liu [b] and Shimin Guo [c]

[a]Institute of Financial Engineering, School of Economics and Commerce, Guangdong University of Technology, Guangzhou, China; [b]Department of business administration, School of Management, Guangdong University of Technology, Guangzhou, China; [c]School of Science, Xi'an Jiaotong University, Xi'an, China

ABSTRACT

This research examines whether there exists an appealing distribution for random jump amplitude, in the sense that with which the stochastic volatility double-jump-diffusions (SVJJ) model would potentially have a superior option market fit, meanwhile keeping a sound balance between reality and tractability. We provide a general methodology for pricing vanilla options, using the Fourier cosine series expansion method (i.e. the COS formula, see [F. Fang and C.W. Oosterlee, *A novel pricing method for European based on Fourier-cosine series expansions*, SIAM J. Sci. Comput. 31 (2008), pp. 826–848], in the setting of Heston's SVJJ (HSVJJ) model that may allow a range of jump amplitude distributions, including the normal distribution, the exponential distribution and the asymmetric double-exponential (db-E) distribution as special cases. An illustrative example examines the implications of HSVJJ model in capturing option 'smirks'. This example highlights the impacts on implied volatility surface of various jump amplitude distributions, through both extensive model calibrations and implied-volatility impacting experiments. Numerical results show that, with the db-E distribution, the HSVJJ model not only captures the implied volatility smile and smirk, but also the 'sadness'.

ARTICLE HISTORY
Received 6 August 2015
Revised 1 December 2015
Accepted 23 January 2016

KEYWORDS
Heston; jump-diffusion; exponential distribution; volatility smile/smirk; volatility sadness; Fourier cosine method

2010 AMS SUBJECT CLASSIFICATIONS
91B70; 91G20; 91G60; 60E10

1. Introduction

Jump-diffusion model, now being widely accepted by academic and industrial world of finance, has witnessed many important innovations in decades. The seminal jump-diffusion model, proposed by [26], faces a serious problem, failing to capture the volatility clustering effects. This problem, however, can be well handled by the stochastic volatility models, such as the Heston model [19], the SABR model [17], the Chen model [7], the GARCH model and so on. Then a natural extension to Merton's jump-diffusion model is a combination of stochastic volatility and jump(s) [8], which thus leads to the stochastic volatility jump-diffusion (SVJ) model, for example, the Bates model [3]. However, effects of return jumps on the future behaviour of asset price are transient, while changes in volatility have an impact on the future distribution of returns [10]. In order to capture both the short- and long-term behaviours of empirically observed financial time series, some Heston-like stochastic volatility double-jump-diffusions (HSVJJ) models were proposed (see, e.g. [9,25]). Furthermore, with regard to the timing of both jumps, the HSVJJ model splits into two branches: HSVIJJ (i.e. double

CONTACT Youfa Sun youfrichsun@gmail.com

jumps arrive independently from each other) and HSVCJJ (i.e. double jumps arrive concurrently; see, e.g. [18,27,30]). While both branches allow large sudden changes in volatility, the SVCJJ model, in particular, links the rapid changes in volatility with times of sudden shocks in the price [10].

Although the SVJJ model has received increasing attention from academia and industry of finance, a quantitative research on the impacts of the type of jump amplitude distribution on market fit seems not so much covered. In canonical literature, the jump amplitude in return was usually assumed to be normally distributed. Then after 2002, the asymmetric double-exponential (db-E) jump assumption became popular (see, e.g. [22,28]), thanks to its properties such as analytical tractability for path-dependent options and capability in capturing the leptokurtic feature of return distribution. Recently, Hanson and coauthors suggested the double-uniform distribution for the return jumps (see, e.g. [34,35]), just because it is the simplest distribution that clearly satisfies the fat-tail property and allows separation of crash and rally behaviours by the double composite property. Though there are still numbers of alternative distribution functions (for example, the t-distribution, the generalized Gaussian function) that can be applied to the jump amplitude, researchers pay little attention to quantitative studies on the impacts of different types of jump-amplitude distribution on market fit. In fact, many interesting topics involving the SVJJ model still remain under investigation, for instance, whether there exists a type of jump amplitude distribution governed by which the SVJJ model can imply a superior market fit to option data; if yes, how about the maintenance (to say, model calibration) of such a double-jump-diffusions model; and how does the combinatorial distributions of double jump sizes affect the market fit.

This research attempts to deal with the above problems, by focusing on the HSVJJ model that may allow a wide range of jump amplitude distributions. Three special distributions, i.e. the normal (N) distribution, the exponential (E) distribution and the asymmetric Db-E distribution, are chosen to be considered, according to the analytical tractability in option pricing and another important criteria that a financial model must have some (economical, physical, psychological, etc.) interpretation [23]. Though we appreciate the uniform-type distributions' good property in generating bounded amplitudes for jump, we do not consider them in this research. The reason is: the uniform distribution is against a common sense that, with irregular and usually non-Markovian event series happened to the real-world market, the resulted jump amplitudes in asset price may be distributed in any ways but uniformly.

Under the HSVJJ models, we develop a general methodology for pricing vanilla European options, applying a Fourier cosine series expansion method (also known as the COS method, see [11]). Then basing on the derived options pricing formula, an illustrative example examines implications of the HSVJJ model in capturing the option market. This example focuses on both the static and dynamic impacts on option 'smirks' of the type of jump amplitude distribution in volatility and return.

In the methodology, this paper generally follows Duffie *et al.* [8] where the impact on option smirks of jump combination, i.e. the normally distributed return jump and exponentially distributed variance jump in the HSVCJJ model, was studied. But beyond this, we expect to screen out an ideal distribution for jump amplitude in the sense that with this distribution, the HSVJJ model would potentially have a superior option market fit. To this, we conduct intensively model calibrations to real options, inspecting the static impacts on implied volatility surfaces of various jump amplitude distributions. Furthermore, we conduct three sets of carefully designed experiments on the capturing capability of the HSVJJ model, inspecting the dynamic impacts on option smirks of transiting the type of jump amplitude distribution from 'A' to 'B'.

In the technique, we choose the COS method, due to its high efficiency as well as excellent accuracy in option pricing (see, e.g. [12]. The COS method, first proposed by Fang and Oosterlee [11], has been widely used to price financial derivatives under asset models that have explicit forms of characteristic function. For instance, it is applied to price the Bermudan options, barrier options [13], swing options [32] and the European-style Asian options [33], under Heston's model [11], under an equity-interest rate hybrid model with stochastic volatility and the interest rate smile [15], under the stochastic volatility models with Hull–White interest rate process [16], and under exponential Lévy

processes [33]. Even though, at this moment no one applies this method to price the vanilla options under both the HSVIJJ and the HSVCJJ model.

In pricing, Ignatieva *et al.* [21] also applied Fourier transform to develop a general methodology for valuing European-style options under the HSVJJ model. Though both are Fourier transformation-based approaches, the COS method is basically different from [21] in the way of numerical calculation. There are also many finite difference schemes and finite element schemes for pricing options under the HSVJJ model, see, e.g. [18] and the references therein. However, we do not suggest these numerical schemes for this research, due to their relatively low efficiency and accuracy, if compared with those of the COS method.

One of interesting findings in this article is: armed with the Db-E jump-size distribution, the HSVJJ model not only captures the empirically observed implied volatility smile and smirk, but also the not so well-known volatility 'sadness'.

2. Financial model

2.1. The model formulation

As an natural extension to the plain Heston stochastic volatility model, the HSVJJ model, under the risk-neutral $\mathbb{Q}$-measure, is defined by an independent variance process and double-jumps feature attaching to the return and variance dynamics, respectively, i.e.

$$\begin{aligned} \mathrm{d}S(t)/S(t^-) &= (r - q - \lambda_s m)\,\mathrm{d}t + \sqrt{v(t^-)}\,\mathrm{d}W^S(t) + (\mathrm{e}^{J_s} - 1)\,\mathrm{d}\pi^s(t), \\ \mathrm{d}v(t) &= \kappa(\theta - v(t^-))\,\mathrm{d}t + \xi\sqrt{v(t^-)}\,\mathrm{d}W^v(t) + J_v\,\mathrm{d}\pi^v(t), \end{aligned} \tag{1}$$

where

- r is the risk-free rate of return, q the yields flow rate, θ the long variance, κ the rate at which $v(t)$ reverts to θ, and ξ the volatility of the volatility that governs the variance of $v(t)$.
- $\pi^s(t)$ is a Poisson process with a constant intensity λ_s (namely the frequency of jumps per year)[1], J_s a random jump size in the logarithm of the asset price with the probability density function (p.d.f) $\varpi(J_s)$. We assume that $\mathbb{E}(\mathrm{e}^{J_s}) < \infty$ for a smooth function ϖ, and let $m = \mathbb{E}(\mathrm{e}^{J_s} - 1)$ to make the discounted asset process a martingale.
- $\pi^v(t)$ is also a Poisson jump process with a constant intensity λ_v and random jump amplitude J_v with the p.d.f $\varpi(J_v)$.
- $W^S(t)$ and $W^v(t)$ are standard Wiener processes with correlation $\langle \mathrm{d}W^S(t),\ \mathrm{d}W^v(t)\rangle = \rho\,\mathrm{d}t$.

The dynamics (1) can be easily specified into the Black–Scholes model, the Merton model, the Heston stochastic volatility model, the Bates' model, the HSVJ model with variance jump, the HSVIJJ model, the HSVCJJ model and so on.

2.2. The jump amplitude distribution

In principle, the HSVJJ model in Equation (1), containing two jump terms, can allow a wide range of jump amplitude distributions, such as the power-type distributions, the exponential-type distributions, the logarithmic-type distributions and their compounded distributions, to mention just a few.

In the space available, however, it would not make sense to discuss all possible distributions, so in what follows a very selective choice will be made, concentration on the analytical tractability for option pricing under the HSVJJ model and economical explanation. As a result, this research considers three important distributions widely appeared in the existing literature, that is, the normal (for convenience of notation, hereinafter, denoted by N) distribution

Table 1. The possible combinations of double-jump amplitude distributions in the HSVJJ model, with elements: the normal (N) distribution, the single-exponential (E) distribution and the Db-E distribution.

(R-J)	(V-J)	(R-J,V-J)	AT	Case#
N		(N,E)	Yes	1
Db-E	E	(Db-E,E)	Yes	2
E		(E,E)	Yes	–
N		(N,Db-E)	Yes	3
Db-E	Db-E	(Db-E,Db-E)	Yes	–
E		(E,Db-E)	Yes	4
N		(N,N)	No	–
Db-E	N	(Db-E,N)	No	–
E		(E,N)	No	–

Note: (R-J) denotes the distribution of jump amplitudes in return; (V-J) that in variance; (R-J,V-J) the combinatorial amplitude distribution of double jumps in the HSVJJ model; and AT the flag of having analytical tractability for standard European options, under the HSVJJ model with given distribution (R-J,V-J).

$\varpi(J) = \exp(-(J-\mu_J)^2/2\sigma_J^2)/\sqrt{2\pi}\sigma_J$ (where J refers to the jump amplitude J_s in return (or J_v in variance)), the single-exponential (E) distribution $\varpi(J) = 1/\eta \exp(-J/\eta) \cdot 1_{J\geq 0}$ where $0 < \eta < 1$, and the Db-E distribution $\varpi(J) = p1/\eta_u \exp(-J/\eta_u) \cdot 1_{J\geq 0} + q1/\eta_d \exp(J/\eta_d) \cdot 1_{J<0}$ where $0 < \eta_u < 1, \eta_d > 0, p > 0, q > 0$ and $p+q=1$.

We do not consider t-distribution, though it is widely used in empirical studies. The reason is that, with t-distribution (or other distributions with power-type tails) as the return distribution, the asset price at the next time may have an unbounded expectation, as long as one considers such models with continuous compounding [22].

Therefore, with above-selected distributions, the possible combinatorial distributions of double jumps in the HSVJJ model are presented in Table 1.

To the best of our knowledge, only a few of these combinations have been studied in the literature. Duffie *et al.*, [8] and D'Ippoliti *et al.* [9] among others, consider the (N,E)-type SVJJ model; Poklewski-Koziell [27] works on both the (N,E) and (N,N)-type SVJJ model. Recently, Zang *et al.* [31] consider numerically the (N,N)-type double-jump stochastic volatility model for VIX. Most of the rest combinations receive no attention from the academic and industrial world of finance. For example, the double-jump combinations that include the Db-E distributed return jump, i.e. (Db-E,E), (Db-E, N) and (Db-E, Db-E), still remain untouched at this moment, though it seems not difficult to extend Kou [23]'s work to them. The underlying reason may be due to a popular viewpoint that a financial model should be parsimonious as possible. But in this research, we need to consider all representative combinations listed in Table 1, to screen out a plausible distribution for jump amplitude in the SVJJ models.

2.3. Leptokurtic feature

The return over a time interval Δt is given by

$$\frac{\Delta S(t)}{S(t)} = \exp\{(r-q-\lambda_s m)\Delta t + \sqrt{v(t)}[W^S(t+\Delta t) - W^S(t)] + \sum_{i=\pi^s(t)+1}^{\pi^s(t+\Delta t)} J_s^i\} - 1, \tag{2}$$

where the summation over an empty set is set to be zero and the variance $v(t)$ is governed by a stochastic volatility jump-diffusion model.

For the HSVJJ model (1), it is extremely complicated to derive an explicit form of return distribution, given the jump amplitudes distributions in return and variance. For convenience, we approximate numerically the return distribution by Monte Carlo method.

In order to make a trade-off between accuracy and efficiency, we apply the famous quadratic exponential (QE) scheme [2], rather than the Euler-based approaches and the exact simulation method (see, e.g [6,14]), to sample the asset and variance processes.

We first partition the time axis with $t = 0, \ldots, T$, with a mesh size $\Delta t = T/N_{\text{parts}}$, and define $\Theta = s_v^2/m_v^2$, where $s_v^2 = \hat{v}(t)\xi^2 e^{-\kappa\Delta t}/\kappa(1 - e^{-\kappa\Delta t}) + \theta\xi^2/2\kappa(1 - e^{-\kappa\Delta t})^2$ and $m_v = \theta + (\hat{v}(t) - \theta)e^{-\kappa\Delta t}$, given the sampled variance $\hat{v}(t)$ at time t. Then the QE scheme, in the context of the HSVJJ model, reads for the variance (for details, please see Andersen [2] and the references therein):

$$\hat{v}(t+\Delta t) = \mathbf{1}_{\Theta \le \Theta_c}[\hat{a}(\hat{b}+Z)^2] + \mathbf{1}_{\Theta > \Theta_c}[\mathbf{1}_{p<U\le 1}\beta^{-1}\log\left(\frac{1-p}{1-U}\right)] + \sum_{i=\pi^v(t)+1}^{\pi^v(t+\Delta t)} J_v^i, \tag{3}$$

where $\Theta_c > 0$ is a constant, $\hat{a} = m_v/1 + \hat{b}^2$, $\hat{b} = 2\Theta^{-1} - 1 + \sqrt{2\Theta^{-1}(2\Theta^{-1} - 1)}$, $p = \Theta - 1/\Theta + 1$, $\beta = 1 - p/m_v$; Z is a standard Gaussian random variable; U a uniform random variable in $[0, 1]$; and J_v^i the amplitude of the ith variance jump happened in the time interval $[t, t + \Delta t]$.

The numerical scheme for the log-price under the HSVJJ model, reads

$$\log(\hat{S}(t+\Delta t)) = \log(\hat{S}(t)) + \left(r - q - \lambda_J m_v\right)\Delta t + K_0 + K_1\hat{v}(t) + K_2\hat{v}(t+\Delta t) + \sqrt{K_3\hat{v}(t) + K_4\hat{v}(t+\Delta t)}Y + \sum_{i=\pi^s(t)+1}^{\pi^s(t+\Delta t)} J_s^i, \tag{4}$$

where $K_0 = -\rho\kappa\theta/\xi\Delta t, K_1 = r_1\Delta t(\kappa\rho/\xi - \frac{1}{2}) - \rho/\xi, K_2 = r_2\Delta t(\kappa\rho/\xi - \frac{1}{2}) + \rho/\xi, K_3 = r_1\Delta t(1-\rho^2), K_4 = r_2\Delta t(1-\rho^2), r_1 + r_2 = 1, r_1, r_2 \in [0, 1]$, Y is a standard Gaussian random variable,

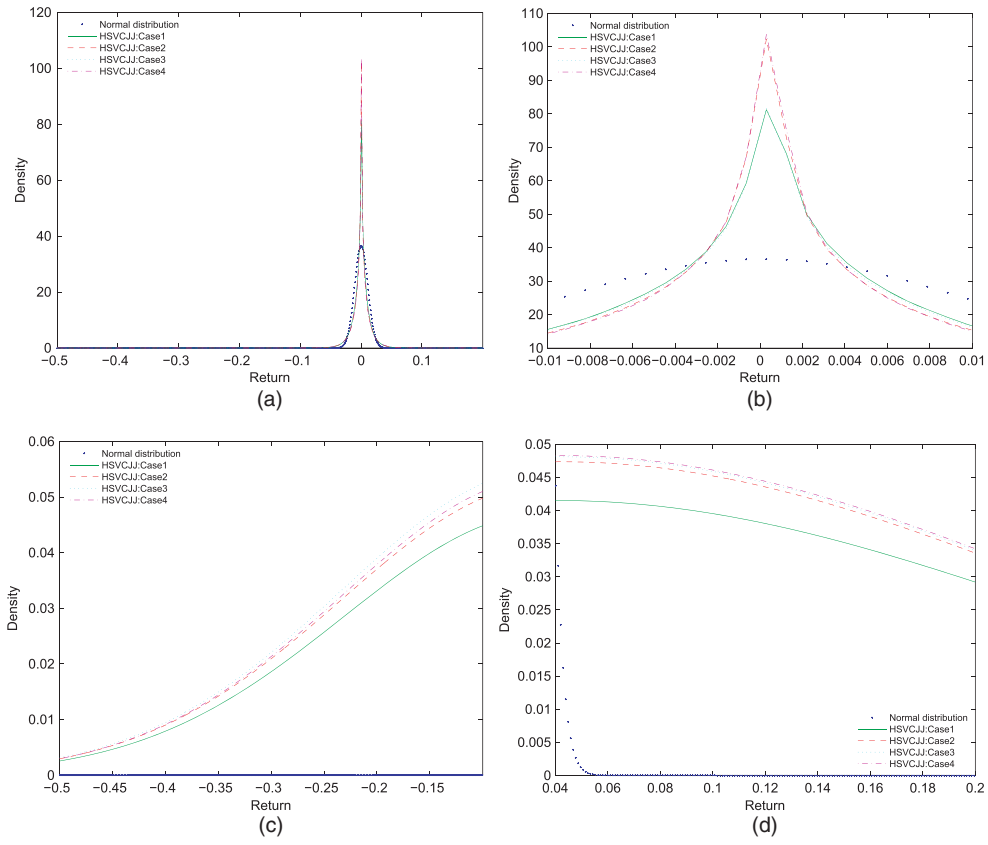

Figure 1. The densities of log-return simulated by the HSVCJJ model with four cases of jump amplitude distributions presented in Table 1, compared with the normal density. (a) The overall shape of the densities, (b) the shape around the peak area, (c) the left tail, and (d) the right tail.

Table 2. Model calibrations to ING Calls.

Case#	Model	Parametrization													MSE
		κ	θ	ξ	ρ	v_0	μ_J	σ_J	λ_s						
	HSVJ	1.6641	0.0650	0.6356	−0.7530	0.0264	0.0457	0.0858	0.1350	η_J	λ_v				1.9821E−4
1	HSVIJJ	1.1145	0.0647	0.5177	−0.7489	0.0297	0.0277	0.0754	0.0771	0.1817	0.0347	ρ_J			1.1765E−4
	HSVCJJ	1.0131	0.0620	0.4980	−0.7210	0.0307	0.0200	0.0183	0.0813	0.1077	0.0183	−0.2722			1.0220E−4
		κ	θ	ξ	ρ	v_0	η_u	η_d	λ_s	p					
	HSVJ	1.3536	0.0695	0.6610	−0.6675	0.0276	0.0366	0.0737	0.1000	0.7586	η_J	λ_v			1.0694E−4
2	HSVIJJ	1.1069	0.0706	0.6015	−0.6754	0.0290	0.0557	0.0721	0.0672	0.6519	0.0224	0.0115	ρ_u	ρ_d	1.0214E−4
	HSVCJJ	1.0670	0.0616	0.5674	−0.5627	0.0302	0.0295	0.0859	0.0631	0.9998	0.1714	0.0631	−0.2034	−0.3499	7.9696E−5
		κ	θ	ξ	ρ	v_0	μ_J	σ_J	λ_s						
	HSVJ	1.6641	0.0650	0.6356	−0.7530	0.0264	0.0457	0.0858	0.1350	η_u	η_d	λ_v	p		1.9821E−4
3	HSVIJJ	1.3106	0.0694	0.7079	−0.6693	0.0244	0.0508	0.0233	0.5153	0.0230	0.4496	0.0113	0.9497	ρ_J	1.0891E−4
	HSVCJJ	1.1695	0.0592	0.5296	−0.7232	0.0290	0.0544	0.0304	0.1759	0.0754	0.2861	0.1759	0.9820	−0.4676	9.7468E−5
		κ	θ	ξ	ρ	v_0	η_J	λ_s							
	HSVJ	1.9065	0.0671	0.8036	−0.6498	0.0339	0.0316	0.0232	η_u	η_d	λ_v	p			2.7623E−4
4	HSVIJJ	1.3000	0.0631	0.6000	−0.7168	0.0278	0.1000	0.0300	0.1000	1.5491	0.1000	0.9873	ρ_J		1.0867E−4
	HSVCJJ	1.1946	0.0659	0.6204	−0.5535	0.0292	0.0510	0.0288	0.1762	1.7534	0.0288	0.9823	−0.2206		8.9802E−5

Note: Case1, i.e. (R-J,V-J) = (N,E), means the case of normally distributed return jumps and the exponentially distributed variance jumps; Case 2: (R-J,V-J) = (Db-E,E); Case 3: (R-J,V-J) = (N,Db-E) and Case 4: (R-J,V-J) = (E,Db-E). HSVJ is the Heston stochastic volatility model with return jumps. The HSVJ model in Case1, means the model with return jumps governed by (R-J) distribution. The rest can be similarly understood.

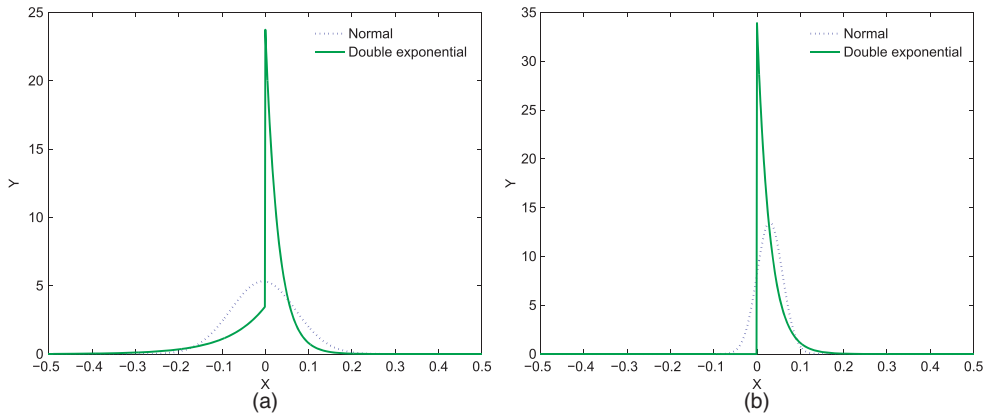

Figure 2. The shapes of double and single-exponential functions, compared to that of normal function with the same mean and variance. For the db-E function, $\eta_u = 0.0295$; $\eta_d = 0.0859$; $p = 0.7$; for the single-exponential function, $\eta = 0.0295$. (a) The double-exponential function, (b) the single-exponential function.

independent of those in the variance processes; and J_s^i the amplitude of the ith return jump happened in the time interval $[t, t + \Delta t]$.

To gain an intuitive understanding to the leptokurtic feature of return distribution driven by the HSVJJ model, we plot the numerical density in Figure 1. In simulation, we use the HSVCJJ model. The parameters are taken from Table 2 in Section 4.1, for coherence. Besides, the number of simulation paths is assigned to 10^5; the duration time is 1-year and $\Delta t = 1/250$ year.

The first panel of Figure 1 compares the overall shapes of the numerical densities simulated by four cases of HSVCJJ models (labelled in Table 1) and the normal density with the average mean and variance of the four. The leptokurtic feature of log-return density is evidently shown in Figure 1(b). The peaks of densities from four models are: 81.2564, 102.3406, 81.7614 and 103.7255, respectively; whereas that of the normal density is 36.5532. The third and fourth panel of Figure 1 display that the densities of return from four models have both heavier right and left tails than the normal density. From Figure 1, we can easily determine that, the leptokurtic feature of the HSVCJJ model of Case 2 (i.e. (R-J, V-J) = (Db-E, E)) and of Case 4 (i.e. (R-J,V-J) = (E, Db-E)), seems slightly more pronounced than that of model of Case 3 (i.e. (R-J, V-J) = (N, Db-E)), whereas the model of Case 1 (i.e. (R-J,V-J) = (N, E)) has the lowest peak and thinnest tails among all four cases.

The inner reason for above ranking is: the Db-E function itself is of strong leptokurtic feature (see Figure 2(a)), which can be inherited by the return distribution of the HSVJJ model; and the shape of single-exponential function is relatively weak leptokurtic (see Figure 2(b)), whereas the normal distribution has no such feature. In Figure 2, the peak ratio of Db-E and N distribution is $\frac{23.7288}{5.3219} = 4.4587$; while the peak ratio of E and N distribution is $\frac{33.8983}{13.5215} = 2.5070$.

At this moment, one can essentially understand why we do not consider the uniform distribution for jump amplitudes in this research. From the shape of density function, the uniform distribution neither exhibits any leptokurtic feature, nor holds normally-fat tails, but has two truncated over-heavy tails. This means, one can hardly image such an insufficient distribution would enhance the HSVJJ model's performance in capturing rightly the empirical characteristics observed in real markets.

3. Option pricing via the COS method

3.1. The COS formula

We apply the Fourier-cosine series expansion method (the COS formula) to value the plain vanilla options under the HSVJJ model. For a detailed description of the COS pricing method under the plain Heston model, please refer to [11].

Given the interest rate r, $\tau = T - t_0$ and $x = \log(S(0)/K), y = \log(S(T)/K)$, the COS formula for plain vanilla European options under the HSVJJ model, reads

$$\hat{V}(t_0, x, v, J_s, J_v) = \mathrm{e}^{-r\tau} \sum_{k=0}^{\prime N-1} \Re\left(\phi\left(\frac{k\pi}{b-a}; x\right) \exp\left(-i\frac{ak\pi}{b-a}\right)\right) U_k, \tag{5}$$

where $\hat{V}(t_0, x, v, J_s, J_v)$ indicates the *approximate option value*, and

$$U_k = \frac{2}{b-a}\int_a^b V(T, y, v) \cos\left(k\pi\frac{y-a}{b-a}\right) \mathrm{d}y, \tag{6}$$

are the Fourier cosine coefficients of $V(T, y, v)$, available in closed form for several payoff functions; notation $\phi(\omega; x)$ (where $\omega = k\pi/(b-a)$) is a short form of $\phi_X(\omega, T; t_0, x, v, J_s, J_v)$, i.e. the conditional characteristic function of y; the integration interval a,b is a truncated domain associated with a Fourier cosine series expansion of transitional density function $\varpi(y|x)$; the prime at the sum-symbol indicates that the first term in the expansion is multiplied by one-half; and $\Re$ means taking the real part of the argument.

3.2. Moment-generating function

As it is well known, the characteristic function $\phi_X(\omega, T; t_0, x, v, J_s, J_v)$ can be directly obtained by substituting $\Omega = i\omega$ into the moment-generating function,

$$G_X(\Omega, T; t_0, x, v, J_s, J_v) \doteq E(\mathrm{e}^{\Omega X_T} | X_{t_0} = x, V_{t_0} = v, J_s, J_v). \tag{7}$$

According to Duffie *et al.* [8] and Sun [29], the moment-generating function has a form of

$$G_X(\Omega, T; t_0, x, v, J_s, J_v) = \mathrm{e}^{\Omega x + P(\tau, \Omega; J_s, J_v) + Q(\tau, \Omega)v}, \tau = T - t_0, \tag{8}$$

where $P(\tau, \Omega; J_s, J_v)$ and $Q(\tau, \Omega)$ are functions to be determined with respect to different jump cases.

By applying Feynman–Kac formula[2], we know $G_X(\cdot)$ solves the following PDE:

$$\begin{aligned} 0 = {} & \frac{\partial f}{\partial t} + \frac{1}{2}v\frac{\partial^2 f}{\partial x^2} + \frac{1}{2}\xi^2 v\frac{\partial^2 f}{\partial v^2} + \rho\xi v\frac{\partial^2 f}{\partial x \partial v} + \left[r - q - \lambda_s m - \frac{1}{2}v\right]\frac{\partial f}{\partial x} + \kappa(\theta - v)\frac{\partial f}{\partial v} \\ & + \begin{cases} \lambda_s \int_{-\infty}^{\infty} (f(x + J_s, v + J_v) - f(x))\varpi(J)\,\mathrm{d}J, & \text{for HSVCJJ} \\ \lambda_s \int_{-\infty}^{\infty} (f(x + J_s) - f(x))\varpi(J_s)\,\mathrm{d}J_s + \lambda_v \int_{-\infty}^{\infty} (f(v + J_v) - f(v))\varpi(J_v)\,\mathrm{d}J_v, \\ \text{for HSVIJJ;} \end{cases} \end{aligned} \tag{9}$$

with the initial condition $f(x, v; \Omega, t_0, J_s, J_v) = \mathrm{e}^{\Omega x}$. In Equation (9), for the case of HSVCJJ model, J is a compound of jumps in volatility and in return, with joint distribution $\varpi(J) = \varpi(J_s|J_v)\varpi(J_v)$.

3.2.1. For the HSVCJJ model.

Substituting Equation (8) into Equation (9), we have the following PDEs:

$$\begin{aligned} \frac{\partial P(\tau, \Omega; J_s, J_v)}{\partial \tau} &= \Omega(r - q)\tau + \kappa\theta Q(\tau, \Omega) + \lambda_s \Lambda(\tau, \Omega; J_s, J_v), \\ \frac{\partial Q(\tau, \Omega)}{\partial \tau} &= \frac{1}{2}\xi^2 Q^2(\tau, \Omega) + (\Omega\rho\xi - \kappa)Q(\tau, \Omega) - \frac{1}{2}(\Omega - \Omega^2), \end{aligned} \tag{10}$$

where $\Lambda(\tau, \Omega; J_s, J_v) = \int_{-\infty}^{\infty} [\int_{-\infty}^{\infty} \mathrm{e}^{\Omega J_s + Q(\tau, \Omega)J_v} \varpi(J_s|J_v)\varpi(J_v)\,\mathrm{d}J_v]\,\mathrm{d}J_s - 1 - \Omega m$.

The above PDEs can be easily solved as below[3] (for more details, please see [20,29])

$$P(\tau,\Omega;J_s,J_v)=\Omega(r-q)\tau+\lambda_s\int_0^\tau\Lambda(\tau',\Omega;J_s,J_v)\,\mathrm{d}\tau'+\frac{\kappa\theta}{2A}\left[-(D+B)\tau-2\ln\left(\frac{1-G\mathrm{e}^{-D\tau}}{1-\Psi}\right)\right],$$
$$Q(\tau,\Omega)=-\frac{D+B}{2A}\frac{1-\mathrm{e}^{-D\tau}}{1-\Psi\mathrm{e}^{-D\tau}}. \tag{11}$$

where $A=\frac{1}{2}\xi^2, B=\xi\rho\Omega-\kappa, C=-\frac{1}{2}(\Omega-\Omega^2), D=\sqrt{B^2-4AC}$ and $\Psi=(B+D)/(B-D)$.

Given the distributions of jump sizes in return and in variance, we can obtain the explicit approximation formula for plain European options if the jump term $\Lambda(\tau,\Omega;J_s,J_v)$ is integrable with respect to τ.

Case 1 $(R-J,V-J)=(N,E)$.

Given $\varpi(J_v)=1/\eta_J\mathrm{e}^{-J_v/\eta_J}\mathbf{1}_{J_v\geq 0}$ and $\varpi(J_s|J_v)=1/\sqrt{2\pi}\sigma_J\mathrm{e}^{-(J_s-\mu_J-\rho_J J_v)^2/2\sigma_J^2}$, where $0<\eta_J<1/\rho_J$ and $\sigma>0$ (such requirements are needed to ensure that $\mathbb{E}(\mathrm{e}^{J_s})<\infty$), we can calculate the integral

$$\int_{-\infty}^{\infty}\left[\int_{-\infty}^{\infty}\mathrm{e}^{\Omega J_s+Q(\tau,\Omega)J_v}\varpi(J_s|J_v)\varpi(J_v)\,\mathrm{d}J_v\right]\mathrm{d}J_s=\frac{\mathrm{e}^{\Omega\mu_J+\frac{1}{2}\Omega^2\sigma_J^2}}{1-\Omega\rho_J\eta_J-\eta_J Q(\tau,\Omega)}; \tag{12}$$

provided that $\Re(1-\Omega\rho_J\eta_J-\eta_J Q(\tau,\Omega))>0$ and

$$m=\mathbb{E}(\mathrm{e}^{J_s}-1)=\frac{\mathrm{e}^{\mu_J+\frac{1}{2}\sigma_J^2}}{1-\rho_J\eta_J}-1. \tag{13}$$

Hence, the conditional moment-generating function can be written as

$$G_X(\Omega,T;t_0,x,v,J_s,J_v)=\exp\left\{\Omega x+\Omega(r-q)\tau+\frac{\kappa\theta}{\xi^2}\left[-(D+B)\tau-2\log\left(\frac{1-\Psi\mathrm{e}^{-D\tau}}{1-\Psi}\right)\right]\right.$$
$$\left.+\frac{v}{\xi^2}\left[-(D+B)\left(\frac{1-\mathrm{e}^{-D\tau}}{1-\Psi\mathrm{e}^{-D\tau}}\right)\right]+\lambda_s\Delta(\tau,\Omega;J_s,J_v)\right\}, \tag{14}$$

where

$$\Delta(\tau,\Omega;J_s,J_v)=\mathrm{e}^{\Omega\mu_J+1/2\Omega^2\sigma_J^2}\left[\frac{\psi_-}{L\psi_--2C\eta_J}\tau+\frac{4C\eta_J}{(DL)^2-(2C\eta_J+BL)^2}\right.$$
$$\left.\cdot\ln\left(1-\frac{L\psi_++2C\eta_J}{2DL}(1-\mathrm{e}^{-D\tau})\right)\right]-(1+\Omega m)\tau \tag{15}$$

and $L=1-\rho_J\eta_J\Omega, \psi_\pm=D\pm B$; A,B,C,D,Ψ are defined in formula (11); and m in formula (13).

Case 2 $(R-J,V-J)=(Db-E,E)$.

Given $\varpi(J_v)=1/\eta_J\mathrm{e}^{-J_v/\eta_J}\mathbf{1}_{J_v\geq 0}$ (where $\eta_J>0$), and $\varpi(J_s|J_v)=p1/\eta_u\mathrm{e}^{-1/\eta_u(J_s-\rho_u J_v)}\mathbf{1}_{J_s\geq\rho_u J_v}+q1/\eta_d\mathrm{e}^{1/\eta_d(J_s-\rho_d J_v)}\mathbf{1}_{J_s\leq\rho_d J_v}$[4] where $0<\eta_u<1,\eta_d>0$ are means of positive and negative jumps, respectively; $p,q\geq 0$ represent the probabilities of positive and negative jumps, $p+q=1$; ρ_u (ρ_d) is a correlation coefficient between the positive (negative) return jumps and variance jumps such that

$\rho_u \geq \rho_d$ and $\rho_u\eta_J < 1$ ($\rho_d\eta_J < 1$), we have

$$\int_{-\infty}^{\infty}\left[\int_{-\infty}^{\infty} \mathrm{e}^{\Omega J_s + Q(\tau,\Omega)J_v}\varpi(J_s|J_v)\varpi(J_v)\,\mathrm{d}J_v\right]\mathrm{d}J_s$$
$$= \frac{p}{(1-\eta_u\Omega)(1-\Omega\rho_u\eta_J-\eta_J Q(\tau,\Omega))} + \frac{q}{(1+\eta_d\Omega)(1-\Omega\rho_d\eta_J-\eta_J Q(\tau,\Omega))}; \tag{16}$$

provided $\Re(1/\eta_u) > \Re(\Omega), \Re(1/\eta_d+\Omega) > 0, \Re(1-\Omega\eta_J\rho_u-\eta_J Q(\tau,\Omega)) > 0, \Re(1-\Omega\eta_J\rho_d-\eta_J Q(\tau,\Omega) > 0)$, and

$$m = \mathbb{E}(\mathrm{e}^{J_s}-1) = \frac{p}{(1-\eta_u)(1-\rho_u\eta_J)} + \frac{q}{(1+\eta_d)(1-\rho_d\eta_J)} - 1. \tag{17}$$

Then, we can easily have the explicit form of $\Delta(\tau,\Omega;J_s,J_v)$ in the conditional moment-generating function (14), that is,

$$\begin{aligned}\Delta(\tau,\Omega;J_s,J_v) = {} & \frac{p}{1-\eta_u\Omega}\left[\frac{\psi_-}{L_u\psi_- - 2C\eta_J}\tau + \frac{4C\eta_J}{(DL_u)^2-(2C\eta_J+BL_u)^2}\right.\\ & \left.\cdot\ln\left(1-\frac{L_u\psi_+ + 2C\eta_J}{2DL_u}(1-\mathrm{e}^{-D\tau})\right)\right] + \frac{q}{1+\eta_d\Omega}\left[\frac{\psi_-}{L_d\psi_- - 2C\eta_J}\tau\right.\\ & \left.+\frac{4C\eta_J}{(DL_d)^2-(2C\eta_J+BL_d)^2}\cdot\ln\left(1-\frac{L_d\psi_+ + 2C\eta_J}{2DL_d}(1-\mathrm{e}^{-D\tau})\right)\right]\\ & -(1+\Omega m)\tau\end{aligned} \tag{18}$$

where $L_u = 1-\rho_u\eta_J\Omega, L_d = 1-\rho_d\eta_J\Omega, \psi_\pm = D\pm B$; A,B,C,D,Ψ are defined in formula (11); and m in formula (17).

Case 3 $(R-J, V-J) = (N, Db-E)$.

Given $\varpi(J_v) = p1/\eta_u\mathrm{e}^{-1/\eta_u J_v}\mathbf{1}_{J_v\geq 0} + q1/\eta_d\mathrm{e}^{1/\eta_d J_v}\mathbf{1}_{J_v<0}$, where $\eta_u > 0, \eta_d > 0$; $p,q \geq 0$ and $p+q=1$; $\varpi(J_s|J_v) = 1/\sqrt{2\pi}\sigma_J\mathrm{e}^{-(J_s-\mu_J-\rho_J J_v)^2/2\sigma_J^2}$, where $\rho_J\eta_u < 1, \rho_J\eta_d > -1$ (such requirements are needed to ensure that $\mathbb{E}(\mathrm{e}^{J_s}) < \infty$); and provided $\Re(Q(\tau,\Omega)\eta_u + \rho_J\eta_u) < 1$ and $\Re(Q(\tau,\Omega)\eta_d + \rho_J\eta_d) > -1$, we have the explicit form of $\Delta(\tau,\Omega;J_s,J_v)$ in the conditional moment-generating function (14),

$$\begin{aligned}\Delta(\tau,\Omega;J_s,J_v) = {} & \mathrm{e}^{\Omega\mu_J+\frac{1}{2}\Omega^2\sigma_J^2}\left\{p\left[\frac{\psi_-}{L_u\psi_- - 2C\eta_u}\tau + \frac{4C\eta_u}{(DL_u)^2-(2C\eta_u+BL_u)^2}\right.\right.\\ & \left.\cdot\ln\left(1-\frac{L_u\psi_+ + 2C\eta_u}{2DL_u}(1-\mathrm{e}^{-D\tau})\right)\right] + q\left[\frac{\psi_-}{L_d\psi_- + 2C\eta_d}\tau\right.\\ & \left.\left.-\frac{4C\eta_d}{(DL_d)^2-(-2C\eta_d+BL_d)^2}\cdot\ln\left(1-\frac{L_d\psi_+ - 2C\eta_d}{2DL_d}(1-\mathrm{e}^{-D\tau})\right)\right]\right\}\\ & -(1+\Omega m)\tau\end{aligned} \tag{19}$$

and $L_u = 1-\rho_J\eta_u\Omega, L_d = 1+\rho_J\eta_d\Omega, \psi_\pm = D\pm B$; A,B,C,D,Ψ are defined in formula (11); and $m = \mathrm{e}^{\mu_J+\frac{1}{2}\sigma_J^2}(p/(1-\rho_J\eta_u) + q/(1+\rho_J\eta_d)) - 1$.

Notice that here $L_d = 1+\rho_J\eta_d\Omega$, is different from the definition of L_d in Case2 where $L_d = 1+\rho_d\eta_J\Omega$.

Case 4 $(R-J, V-J) = (E, Db-E)$.

Given $\varpi(J_v) = p1/\eta_u\mathrm{e}^{-1/\eta_u J_v}\mathbf{1}_{J_v\geq 0} + q1/\eta_d\mathrm{e}^{1/\eta_d J_v}\mathbf{1}_{J_v<0}$, where $\eta_u > 0, \eta_d > 0$; $p,q \geq 0$ and $p+q=1$, $\varpi(J_s|J_v) = 1/\eta_J\mathrm{e}^{-1/\eta_J(J_s-\rho_J J_v)}\mathbf{1}_{J_s\geq\rho_J J_v}$ where $\eta_J > 0$; ρ_J is a correlation coefficient between the return jumps and variance jumps such that $\rho_J\eta_u < 1$ and $\rho_J\eta_d > -1$; and provided

$\Re(1-\eta_J\Omega)>0, \Re(Q(\tau,\Omega)\eta_u+\rho_J\eta_u)<1, \Re(Q(\tau,\Omega)\eta_d+\rho_J\eta_d)>-1$, we have the explicit form of $\Delta(\tau,\Omega;J_s,J_v)$ in the conditional moment-generating function (14), that is,

$$\begin{aligned}\Delta(\tau,\Omega;J_s,J_v) = {} & \frac{p}{1-\eta_J\Omega}\left[\frac{\psi_-}{L_u\psi_- - 2C\eta_u}\tau + \frac{4C\eta_u}{(DL_u)^2-(2C\eta_u+BL_u)^2}\right.\\ & \left.\cdot \ln\left(1-\frac{L_u\psi_+ + 2C\eta_u}{2DL_u}(1-\mathrm{e}^{-D\tau})\right)\right] + \frac{q}{1-\eta_J\Omega}\left[\frac{\psi_-}{L_d\psi_- + 2C\eta_d}\tau\right.\\ & \left.-\frac{4C\eta_d}{(DL_d)^2-(-2C\eta_d+BL_d)^2}\cdot\ln\left(1-\frac{L_d\psi_+ - 2C\eta_d}{2DL_d}(1-\mathrm{e}^{-D\tau})\right)\right]\\ & -(1+\Omega m)\tau, \end{aligned} \tag{20}$$

where $L_u = 1-\rho_J\eta_u\Omega, L_d = 1+\rho_J\eta_d\Omega, \psi_\pm = D\pm B$; A,B,C,D,Ψ are defined in formula (11); and $m = p/(1-\eta_u\rho_J)+q/(1+\eta_d\rho_J)-1$.

Remark 1 (On moment-generating function of other five cases)**:** Except for the above four cases of combinatorial distributions of double jumps, there are two trivial cases, to say, $(R-J,V-J) = (Db-E,Db-E)and(R-J,V-J) = (E,E)$, that we can easily derive the moment-generating functions, following the above procedures. However, including these two cases brings no extra insights to this research.

Moreover, for the rest of three cases, i.e. (N, N), (E, N) and (Db-E, N), due to no explicit form for the integral

$$\int_0^\tau \mathrm{e}^{0.5(\Omega\rho_J+Q(\tau',\Omega))^2+\nu_J(\Omega\rho_J+Q(\tau',\Omega))}\,\mathrm{d}\tau',$$

given $\varpi(J_v) = 1/\sqrt{2\pi}\sigma_J\mathrm{e}^{-(J_v-\nu_J)^2/2\sigma_J^2}$, we cannot obtain the explicit form of $\Delta(\tau,\Omega;J_s,J_v)$ for the conditional moment-generating function (14). Thus we do not consider these cases in this paper. But please note that, discarding the above three cases would not sacrifice insights much for this research, since we have already considered two HSVJJ models with normally distributed jumps, that is, Case1:$(R-J,V-J) = (N,E)$ and Case3:$(R-J,V-J) = (N,Db-E)$.

Accordingly, we neither consider the above five cases for the HSVIJJ models in the forthcoming section.

3.2.2. For the HSVIJJ model.

Given the return jumps and variance jumps arrive independently, we have PDEs for the HSVIJJ model

$$\begin{aligned}\frac{\partial P(\tau,\Omega;J_s,J_v)}{\partial\tau} &= \Omega(r-q)\tau+\kappa\theta Q(\tau,\Omega)+\lambda_s\Lambda_s(\tau,\Omega;J_s)+\lambda_v\Lambda_v(\tau,\Omega;J_v),\\ \frac{\partial Q(\tau,\Omega)}{\partial\tau} &= \frac{1}{2}\xi^2Q^2(\tau,\Omega)+(\Omega\rho\xi-\kappa)Q(\tau,\Omega)-\frac{1}{2}(\Omega-\Omega^2),\end{aligned} \tag{21}$$

where $\Lambda_s(\tau,\Omega;J_s) = \int_{-\infty}^{\infty}\mathrm{e}^{\Omega J_s}\varpi(J_s)\,\mathrm{d}J_s - 1-\Omega m$ and $\Lambda_v(\tau,\Omega;J_v) = \int_{-\infty}^{\infty}\mathrm{e}^{Q(\tau,\Omega)J_v}\varpi(J_v)\,\mathrm{d}J_v - 1$.

The above PDEs can be solved as below,

$$\begin{aligned}P(\tau,\Omega;J_s,J_v) &= \Omega(r-q)\tau+\frac{\kappa\theta}{2A}\left[-(D+B)\tau-2\ln\left(\frac{1-G\mathrm{e}^{-D\tau}}{1-\Psi}\right)\right]\\ &\quad+\lambda_s\int_0^\tau\Lambda_s(\tau',\Omega;J_s)\,\mathrm{d}\tau'+\lambda_v\int_0^\tau\Lambda_v(\tau',\Omega;J_v)\,\mathrm{d}\tau';\\ Q(\tau,\Omega) &= -\frac{D+B}{2A}\frac{1-\mathrm{e}^{-D\tau}}{1-\Psi\mathrm{e}^{-D\tau}}.\end{aligned}$$

3.2.2.1. Case 1: $(R-J, V-J) = (N, E)$. Given $\varpi(J_v) = 1/\eta_J e^{-J_v/\eta_J}\mathbf{1}_{J_s\geq 0}$ where $\eta_J > 0$ and $\varpi(J_s) = 1/\sqrt{2\pi}\sigma_J e^{-(J_s-\mu_J)^2/2\sigma_J^2}$, we can calculate the integral

$$\int_{-\infty}^{\infty} e^{\Omega J_s}\varpi(J_s)\,dJ_s = e^{\Omega\mu_J+1/2\Omega^2\sigma_J^2}; \tag{22}$$

$$\int_{-\infty}^{\infty} e^{Q(\tau,\Omega)J_v}\varpi(J_v)\,dJ_v = \frac{1}{1-Q(\tau,\Omega)\eta_J}; \tag{23}$$

provided $\Re(1-Q(\tau,\Omega)\eta_J > 0)$ and

$$m = \mathbb{E}(e^{J_s}-1) = \int_{-\infty}^{\infty} e^{J_s}\varpi(J_s)\,dJ_s - 1 = e^{\mu_J+1/2\sigma_J^2} - 1. \tag{24}$$

Hence, the conditional moment-generating function can be written

$$\begin{aligned} G_X(\Omega,T;t_0,x,v,J_s,J_v) = \exp\Bigg\{&\Omega x + \Omega(r-q)\tau + \frac{\kappa\theta}{\xi^2}\left[-(D+B)\tau - 2\log\left(\frac{1-\Psi e^{-D\tau}}{1-\Psi}\right)\right] \\ &+ \frac{v}{\xi^2}\left[-(D+B)\left(\frac{1-e^{-D\tau}}{1-\Psi e^{-D\tau}}\right)\right] + \lambda_s\Delta_s(\tau,\Omega;J_s) + \lambda_v\Delta_v(\tau,\Omega;J_v)\Bigg\}, \end{aligned} \tag{25}$$

where

$$\Delta_s(\tau,\Omega;J_s) = \left(e^{\Omega\mu_J+\frac{1}{2}\Omega^2\sigma_J^2} - 1 - \Omega m\right)\tau, \tag{26}$$

$$\Delta_v(\tau,\Omega;J_v) = \frac{\psi_-}{\psi_- - 2C\eta_J}\tau + \frac{4C\eta_J}{(D)^2-(2C\eta_J+B)^2}\ln\left[1-\frac{\psi_+ + 2C\eta_J}{2D}(1-e^{-D\tau})\right] - \tau, \tag{27}$$

where m is defined in formula (24).

3.2.2.2. Case 2: $(R-J, V-J) = (Db-E, E)$. Given $\varpi(J_v) = 1/\eta_J e^{-J_v/\eta_J}\mathbf{1}_{J_s\geq 0}$ where $\eta_J > 0$ and $\varpi(J_s) = p1/\eta_u e^{-1/\eta_u J_s}\mathbf{1}_{J_s\geq 0} + q1/\eta_d e^{1/\eta_d J_s}$
$\mathbf{1}_{J_s<0}$, where $0 < \eta_u < 1$ and $\eta_d > 0$, and provided $\Re(1/\eta_u) > \Re(\Omega)$ and $\Re(1/\eta_d + \Omega) > 0$, we have the explicit form of $\Delta_s(\tau,\Omega;J_s)$ in the conditional moment-generating function (24),

$$\Delta_s(\tau,\Omega;J_s) = \left(\frac{p}{1-\eta_u\Omega} + \frac{q}{1+\eta_d\Omega} - 1 - \Omega m\right)\tau, \tag{28}$$

where $m = p/(1-\eta_u) + q/(1+\eta_d) - 1$, and $\Delta_v(\tau,\Omega;J_v)$ in formula (27).

3.2.2.3. Case 3: $(R-J, V-J) = (N, Db-E)$. Given $\varpi(J_v) = p1/\eta_u e^{-1/\eta_u J_v}\mathbf{1}_{J_v\geq 0} + q1/\eta_d e^{1/\eta_d J_v}$ $\mathbf{1}_{J_v<0}$ (where $\eta_u > 0, \eta_d > 0$) and $\varpi(J_s) = 1/\sqrt{2\pi}\sigma_J e^{-(J_s-\mu_J)^2/2\sigma_J^2}$, and provided $\Re(1-\eta_u\Omega) > 0$ and $\Re(1+\eta_d\Omega) > 0$, we have the explicit form of $\Delta_s(\tau,\Omega;J_s)$ and $\Delta_v(\tau,\Omega;J_v)$ in the conditional moment-generating function (24),

$$\Delta_s(\tau,\Omega;J_s) = \left(e^{\Omega\mu_J+1/2\Omega^2\sigma_J^2} - 1 - \Omega m\right)\tau, \tag{29}$$

$$\begin{aligned} \Delta_v(\tau,\Omega;J_v) = p\Bigg[&\frac{\psi_-}{\psi_- - 2C\eta_u}\tau + \frac{4C\eta_u}{(D)^2-(2C\eta_u+B)^2} \\ &\cdot \ln\left(1-\frac{\psi_+ + 2C\eta_u}{2D}(1-e^{-D\tau})\right)\Bigg] + q\Bigg[\frac{\psi_-}{\psi_- + 2C\eta_d}\tau \end{aligned}$$

$$-\frac{4C\eta_d}{(D)^2-(-2C\eta_d+B)^2}\cdot\ln\left(1-\frac{\psi_+-2C\eta_d}{2D}(1-\mathrm{e}^{-D\tau})\right)\Bigg]-\tau, \tag{30}$$

where $m=\mathrm{e}^{\mu_J+\frac{1}{2}\sigma_J^2}-1$.

3.2.2.4. Case 4: $(R-J,V-J)=(E,Db-E)$. Given $\varpi(J_v)=p1/\eta_u\mathrm{e}^{-1/\eta_u J_v}\mathbf{1}_{J_v\geq 0}+q1/\eta_d\mathrm{e}^{1/\eta_d J_v}\mathbf{1}_{J_v<0}$ (where $\eta_u>0,\eta_d>0$) and $\varpi(J_s)=1/\eta_J\mathrm{e}^{-1/\eta_J J_s}\mathbf{1}_{J_s\geq 0}$ (where $0<\eta_J<1$), and provided $\Re(1-\eta_J\Omega)>0;\Re(1-\eta_u\Omega)>0$ and $\Re(1+\eta_d\Omega)>0$, we have the explicit form of $\Delta_s(\tau,\Omega;J_s)$ in the conditional moment-generating function (24),

$$\Delta_s(\tau,\Omega;J_s)=\left(\frac{1}{1-\eta_J\Omega}-1-\Omega m\right)\tau, \tag{31}$$

where $m=1/1-\eta_J-1$ and $\Delta_v(\tau,\Omega;J_v)$ in formula (27).

3.3. The calculation of integration interval [a, b]

Integration interval variables a and b are determined, so that

$$\int_{\Re}\varpi(y|x)\,\mathrm{d}y-\int_a^b\varpi(y|x)\,\mathrm{d}y<TOL. \tag{32}$$

According to Fang and Oosterlee [11], a and b is given by

$$a=c_1-L_{\cos}\sqrt{c_2+\sqrt{c_4+\sqrt{c_6+\sqrt{c_8+\ldots}}}};\quad b=c_1+L_{\cos}\sqrt{c_2+\sqrt{c_4+\sqrt{c_6+\sqrt{c_8+\ldots}}}}, \tag{33}$$

where c_1 and c_{2k} $(k=1,2,3,\ldots)$ is the first and the $2k$th-order cumulant, respectively, and $L_{\cos}(L_{\cos}>0)$ is a proportional constant. Fang and Oosterlee [11] suggest that including the 4th-order cumulant is sufficient to obtain a good integration interval for the COS method. Larger values of parameter $L_{\cos}$ would correspond to larger N, i.e. the number of truncation terms in formula (5). For example, $L_{\cos}=20$ and $N=200$ are taken in this research.

Due to the limit of space, we only take Case1 (i.e. $(R-J,V-J)=(N,E)$) for example, and provide here only the first and second cumulant, while omitting the lengthy 4th-order cumulant.[5]

For the HSVCJJ, we have

$$c_1=x+\left(r-q-\frac{\theta}{2}\right)\tau+\frac{\theta-v}{2\kappa}(1-\mathrm{e}^{-\kappa\tau})+\lambda_s\left[\mu_J+\eta_J\rho_J+\frac{\mathrm{e}^{\mu_J+0.5\sigma_J^2}}{\eta_J\rho_J-1}+1-\frac{\eta_J}{2\kappa}\right]\tau, \tag{34}$$

$$c_2=\frac{1}{8\kappa^3}\left(\Gamma_0+\Gamma_1\mathrm{e}^{-\kappa\tau}+\Gamma_2\mathrm{e}^{-\kappa_2\tau}\right)+\lambda_s\Upsilon\tau, \tag{35}$$

with

$$\Gamma_0=(2\kappa\theta\tau-5\theta+2v)\xi^2+8\rho[-\kappa^2\theta\tau+\kappa(2\theta-v)]\xi+8\kappa^3\theta\tau-8(\theta-v)\kappa^2;$$

$$\Gamma_1=[4\kappa(\theta-v)\tau+4\theta]\xi^2-8\rho[\kappa^2(\theta-v)\tau+\kappa(2\theta-v)]\xi+8\kappa^2(\theta-v);$$

$$\Gamma_2=(\theta-2v)\xi^2;$$

$$\Upsilon=(\mu_J^2+\rho_J^2+2\eta_J\rho_J\mu_J+2\eta_J^2\rho_J^2)+\frac{\eta_J}{\kappa}(1-\mu_J-2\eta_J\rho_J)+\frac{\eta_J}{\kappa^2}(-\rho\xi+0.5\eta_J)+0.25\frac{\eta_J}{\kappa^3}\xi^2.$$

For the HSVIJJ, we find that

$$c_1 = x + \left(r - q - \frac{\theta}{2}\right)\tau + \frac{\theta - v}{2\kappa}(1 - \mathrm{e}^{-\kappa\tau}) + \left[\lambda_s(\mu_J + \mathrm{e}^{\mu_J + 0.5\sigma_J^2} + 1) - \lambda_v \frac{\eta_J}{2\kappa}\right]\tau; \tag{36}$$

$$c_2 = \frac{1}{8\kappa^3}\left(\Gamma_0 + \Gamma_1 \mathrm{e}^{-\kappa\tau} + \Gamma_2 \mathrm{e}^{-\kappa_2\tau}\right) + (\lambda_s \Upsilon_1 + \lambda_v \Upsilon_2)\tau, \tag{37}$$

with:

$$\begin{aligned}
\Gamma_0 &= (2\kappa\theta\tau - 5\theta + 2v)\xi^2 + 8\rho[-\kappa^2\theta\tau + \kappa(2\theta - v)]\xi + 8\kappa^3\theta\tau - 8(\theta - v)\kappa^2;\\
\Gamma_1 &= [4\kappa(\theta - v)\tau + 4\theta]\xi^2 - 8\rho[\kappa^2(\theta - v)\tau + \kappa(2\theta - v)]\xi + 8\kappa^2(\theta - v);\\
\Gamma_2 &= (\theta - 2v)\xi^2;\\
\Upsilon_1 &= \sigma_J^2 + \mu_J^2;\\
\Upsilon_2 &= \frac{\eta_J}{\kappa} + \frac{\eta_J}{\kappa^2}(-\rho\xi + 0.5\eta_J) + 0.25\frac{\eta_J}{\kappa^3}\xi^2.
\end{aligned}$$

Remark 2: Notice that one cannot obtain Υ_1 and Υ_2 by simply substituting $\rho_J = 0$ into the Υ formula. This can be easily seen from their own generating function (14) and (24).

Though lengthy these cumulants are, they can be easily treated, using Mathematica or Matlab. Hence, given a parameter $L_{\cos}$, integration domain $[a, b]$ in Equation (30) can be determined.

Remark 3 (On the performance of the COS method)**:** There are dozens of papers, published by Professor C. W. Ooesterlee and his teams that have reported the accuracy and speed of the COS method for pricing options since 2008. Nowadays, the COS method is becoming one of alternative tools to provide the reference values for some options (see, e.g. [11,29]).

For a fast glance at the COS method's performance in option pricing, here we show some numerical results on a benchmark problem [6]) under the plain Heston model, i.e.

$$\begin{aligned}
\mathrm{d}S(t)/S(t^-) &= r\,\mathrm{d}t + \sqrt{v(t^-)}\,\mathrm{d}W^S(t),\\
\mathrm{d}v(t) &= \kappa(\theta - v(t^-))\,\mathrm{d}t + \xi\sqrt{v(t^-)}\,\mathrm{d}W^v(t),
\end{aligned}$$

with $S_0 = 100, K = 100, v_0 = 0.09, \kappa = 2.00, \theta = 0.09, \xi = 1.0, \rho = -0.30, r = 0.05, T = 5.0,$ and the true value 34.9998. In implementation, we take $L_{\cos} = 20$ and $N = 200$ for the COS method. The log error between the option price calculated with the COS method and the reference is -4.3804, the CPU time is 6.8784×10^{-3} s.[6]

Given the HSVCJJ model in case1 with parameters recorded in Table 2, the CPU time for pricing a European option is 0.0413 seconds.

4. Implication

4.1. Model calibration

Consider that we have M expiries $T^j (j = 1, 2, \ldots, M)$, and for each maturity T^j, we have N^j calibrating instruments, with strikes K_{ij}, for which market data is given (as prices or implied volatilities). In this

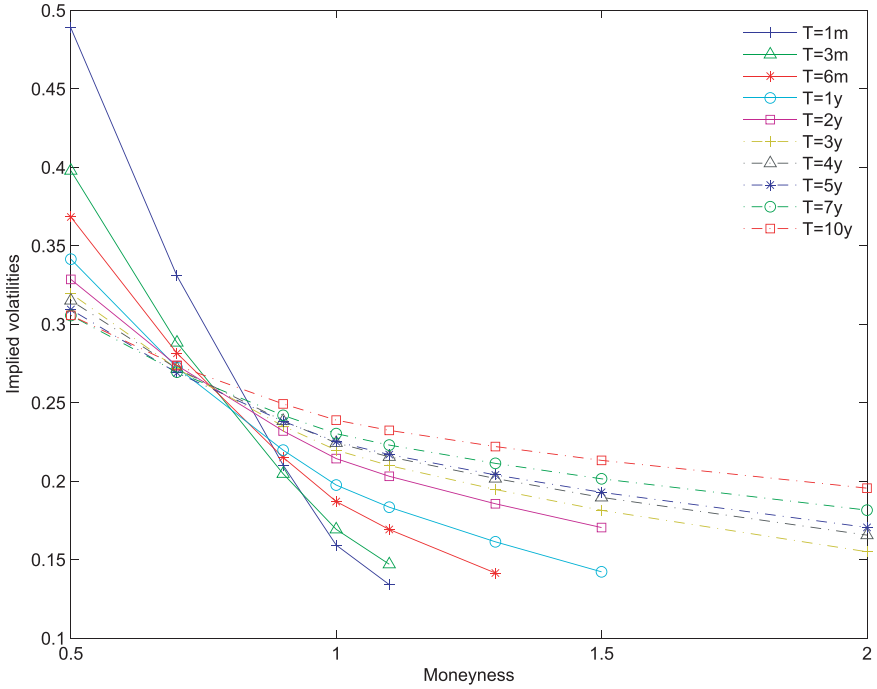

Figure 3. The quoted implied volatilities surfaces of ING European calls of ten different maturities, on January 12, 2005.

paper, the calibration function is defined as the Mean Square Error (MSE), i.e.

$$\mathrm{MSE} = \frac{1}{M}\sum_{j=1}^{M}\left[\frac{1}{N^j}\sum_{i=1}^{N^j}\left(ModelOutput(i,T^j) - MarketData(i,T^j)\right)^2\right], \tag{38}$$

where the *ModelOutput* refers to the implied volatility. The parameters are then estimated by minimizing the MSE.[7] Though the indirect calibration approach is not strictly justified, this is a common procedure at this moment. For details, please see, e.g. [24,29].

A total of 70 ING call options, observed on 12 January 2005, are used. The option implied volatility surfaces are displayed in Figure 3.

Remark 4 (On model calibration to ING options)**:** (1) ING options on ING stock, traded in NYSE, are typically American-style options. The ING option data quoted here are the implied volatilities transformed from American option prices. There are many models available for calculating the implied volatility of an American option. One of popular methods, employed by ***OptionMetrics***, is the Cox–Ross–Rubinstein model. However, this method involves intensive numerical calculations which prevent it from running on a Laptop if the implied volatilities on a hundreds of option contracts are required. The most efficient closed-form approximation appears to be Bjerksund and Stensland [5], which is recommended by Matlab as the top choice for American options. The command 'impvbybjs' in Matlab computes the implied volatility of American options with continuous dividend yield, using the Bjerksund–Stensland option pricing model. For more details, please see [4,5].

(2) We noticed that a few of papers have discussed the calibration directly with American options, see, e.g. [1]. Strictly, we should do this for model calibration. However, the complicate algorithm involved there, seems beyond the scope of this research.

Table 3. Recalibration of the HSVCJJ models in 10 independent runs.

Case#	*Parameter*	No.1	No.2	No.3	No.4	No.5	No.6	No.7	No.8	No.9	No.10
	κ	1.0005	1.0702	1.0687	1.0502	1.0001	1.1155	1.0064	1.0355	1.0905	1.0544
	θ	0.0641	0.0613	0.0628	0.0621	0.0652	0.0633	0.0652	0.0672	0.0645	0.0661
	ξ	0.4979	0.5050	0.4896	0.5166	0.5467	0.5264	0.5208	0.5326	0.5181	0.5523
	ρ	−0.7240	−0.6988	−0.7434	−0.6835	−0.6692	−0.7236	−0.7026	−0.6832	−0.7212	−0.6839
	v_0	0.0308	0.0296	0.0312	0.0315	0.0313	0.0307	0.0305	0.0312	0.0311	0.0304
1	μ_J	0.0314	0.0127	0.0142	0.0168	0.0159	0.0204	0.0192	0.0202	0.0212	0.0201
	σ_J	0.0195	0.0121	0.0100	0.0231	0.0166	0.0114	0.0181	0.0189	0.0169	0.0211
	λ_s	0.0706	0.0897	0.0683	0.0853	0.0733	0.0707	0.0687	0.0531	0.0688	0.0549
	η_J	0.1114	0.1003	0.1182	0.0918	0.0895	0.1049	0.0978	0.0919	0.0918	0.1000
	λ_v	0.0706	0.0897	0.0683	0.0853	0.0733	0.0707	0.0687	0.0531	0.0688	0.0549
	ρ_J	−0.2835	−0.3086	−0.2012	−0.3514	−0.3783	−0.2752	−0.3415	−0.3833	−0.3904	−0.3466
	RME	1.0371E−4	1.0142E−4	1.0442E−4	1.0367E−4	1.0294E−4	1.0197E−4	9.9733E−5	1.0382E−4	1.0253E−4	1.0047E−4
	κ	1.1442	1.0683	1.1546	1.1705	1.1895	1.0328	1.0135	1.1107	1.1163	1.1002
	θ	0.065	0.0618	0.0665	0.0627	0.062	0.0653	0.0662	0.0604	0.0653	0.0619
	ξ	0.6047	0.5553	0.6122	0.5898	0.5932	0.5833	0.5965	0.5694	0.5894	0.5739
	ρ	−0.6148	−0.5438	−0.6487	−0.5389	−0.5915	−0.6259	−0.5486	−0.5353	−0.6248	−0.5378
	v_0	0.0297	0.0299	0.0293	0.0296	0.03	0.0301	0.0301	0.0299	0.0297	0.0298
	η_u	0.0333	0.02	0.0415	0.033	0.0392	0.0366	0.0205	0.02	0.0641	0.0201
2	η_d	0.0457	0.0714	0.0432	0.0614	0.04	0.0845	0.0422	0.0469	0.0152	0.0527
	λ_s	0.0437	0.0531	0.0543	0.0426	0.055	0.0595	0.0427	0.0624	0.0446	0.0561
	p	0.9957	0.9882	0.932	0.9636	0.9154	0.9818	0.958	0.9742	0.8312	0.9399
	η_J	0.187	0.1836	0.1372	0.1941	0.1781	0.1417	0.2026	0.1859	0.1736	0.1755
	λ_v	0.0437	0.1687	0.0543	0.2226	0.1484	0.0595	0.0427	0.3948	0.0446	0.3952
	ρ_u	−0.178	−0.2097	−0.1696	−0.2605	−0.1909	−0.1622	−0.2292	−0.1916	−0.177	−0.2059
	ρ_d	−0.437	−0.4331	−0.2218	−0.3913	−0.3692	−0.4391	−0.3172	−0.4096	−0.3626	−0.4649
	RME	8.35E−05	9.15E−05	8.86E−05	9.45E−05	8.61E−05	8.58E−05	8.27E−05	9.12E−05	8.56E−05	9.04E−05
	κ	1.0284	1.2359	1.1143	1.1562	1.1892	1.1404	1.2632	1.2353	1.1695	1.2120
	θ	0.0646	0.0651	0.0632	0.0634	0.0631	0.0637	0.0631	0.0656	0.0592	0.0621
	ξ	0.5903	0.6212	0.5677	0.6100	0.5860	0.6076	0.6268	0.5551	0.5296	0.6167
	ρ	−0.6071	−0.6497	−0.6801	−0.6248	−0.6693	−0.6209	−0.6418	−0.6444	−0.7232	−0.6736
	v_0	0.0288	0.0277	0.0292	0.0280	0.0291	0.0290	0.0276	0.0291	0.0290	0.0269
	μ_J	0.0439	0.0388	0.0433	0.0308	0.0549	0.0316	0.0451	0.0023	0.0544	0.0688

3	σ_J	0.0263	0.0351	0.0273	0.0384	0.0246	0.0220	0.0215	0.0154	0.0304	0.0289
	λ_s	0.1270	0.1150	0.1294	0.1437	0.1116	0.1340	0.1551	0.0193	0.1759	0.1339
	η_u	0.0741	0.0645	0.0717	0.0691	0.0828	0.0771	0.0656	0.2039	0.0754	0.0834
	η_d	0.1873	0.3433	0.3579	0.2903	0.2011	0.3591	0.2516	0.8432	0.2861	0.2836
	λ_v	0.1270	0.1150	0.1294	0.1437	0.1116	0.1340	0.1551	0.0193	0.1759	0.1339
	p	0.9385	0.9606	0.9770	0.9615	0.9586	0.9671	0.9558	0.9133	0.9820	0.9760
	ρ_J	−0.5886	−0.4849	−0.5712	−0.5105	−0.4711	−0.3714	−0.5976	−0.0287	−0.4676	−0.4315
	RME	9.3706E−05	9.9504E−05	9.8915E−05	9.2866E−05	9.5451E−05	9.4926E−05	9.5247E−05	9.6243E−05	9.7468E−05	9.7682E−05
	κ	1.1010	1.0988	1.1219	1.0548	1.0948	1.0807	1.0948	1.1671	1.1281	1.1130
	θ	0.0655	0.0659	0.0701	0.0693	0.0664	0.0697	0.0664	0.0670	0.0686	0.0664
	ξ	0.5941	0.5908	0.6647	0.6500	0.5943	0.6157	0.5943	0.6195	0.5784	0.6004
	ρ	−0.5520	−0.5548	−0.5547	−0.5348	−0.5549	−0.6128	−0.5549	−0.5553	−0.6563	−0.5548
	v_0	0.0295	0.0296	0.0292	0.0299	0.0296	0.0297	0.0296	0.0294	0.0295	0.0295
4	η_J	0.0275	0.0321	0.0301	0.0350	0.0314	0.0407	0.0314	0.0455	0.0266	0.0327
	λ_s	0.0674	0.0418	0.0424	0.0466	0.0447	0.0375	0.0447	0.0356	0.0352	0.0484
	η_u	0.0816	0.1309	0.0755	0.1094	0.1114	0.0865	0.1114	0.0978	0.1155	0.0982
	η_d	1.2313	1.3417	1.7008	1.9744	1.2235	1.4954	1.2235	1.2208	1.5248	1.2628
	λ_v	0.0674	0.0418	0.0424	0.0466	0.0447	0.0375	0.0447	0.0356	0.0352	0.0484
	p	0.9934	0.9896	0.9999	0.9799	0.9897	0.9749	0.9897	0.9888	0.9641	0.9895
	ρ_J	−0.5273	−0.2503	−0.6656	−0.1901	−0.3470	−0.3933	−0.3470	−0.4838	−0.3057	−0.4217
	RME	8.7001E−05	8.6955E−05	8.4199E−05	8.5272E−05	8.6690E−05	9.0601E−05	8.6690E−05	8.7795E−05	9.1123E−05	8.6336E−05

Note: Case 1 denotes the combinatorial distributions of normally distributed return jumps and the exponentially distributed variance jumps, i.e. Case 1: (R-J,V-J) = (N,E); Case 2: (R-J,V-J) = (Db-E,E); Case 3: (R-J,V-J) = (N,Db-E) and Case 4: (R-J,V-J) = (E,Db-E).

(3) The reason why we consider an individual stock option rather than a European-style Index option is that: the latter may imply much more profound volatility patterns. These rich patterns are exactly what we need to screen out an appealing distribution from a given set such that with this distribution for jump amplitudes, the SVJJ model would achieve a superior market fit.

The risk-free rate was assumed to be fixed at $r = 3.06\%$ on that particular day, and the dividend yield at $q = 0$. Rather than estimating the initial value of stochastic volatility on the sample day, we treat it as one of parameters to be calibrated.

Table 2 records the calibrated parameters of the HSVJ, HSVIJJ and HSVCJJ models. Table 3 provides 10-independent-run recalibration results for the HSVCJJ models, to show both the convenience and robust of model parametrization.

Table 2 provides us the following insights on the significance of jump-size distribution type to the jump-diffusion models:

- The HSVJ model, with return-jump amplitudes governed by the Db-E distribution, outperforms models with jumps governed by the N distribution and the single E distribution, having the best overall market fit to the option data.
- Among four cases of the HSVJJ (including both HSVIJJ and HSVCJJ) models, the models with double-jump amplitudes governed by pure exponential-type combinatorial distributions, i.e. Case2 (Db-E,E) and Case4 (E, Db-E), have slightly better overall fits than the models by db-E-normal mixed distributions, i.e. Case3 (N, Db-E), while the HSVJJ model with jumps governed by single-exponential-normal mixed distributions, i.e. Case1 (N,E), has the worst market fit.

Remark 5 (On the fit rankings)**:** (1) One may attribute the above fit rankings to the scale of parameters in HSVJJ models and take it for granted that the more parameters a model has the better market fit it possesses. He/she should notice that the HSVIJJ model in case 1 has more parameters than the HSVJ model in case 2, but the former model does not have a better market fit. There are another two evidence: (1) the HSVCJJ models in case 2 (Db-E,E) and Case 3 (N, Db-E) have the same number of parameters (see Table 2), but their market fits are quite different, with case 2 outperforming case 3 dramatically; (2) the HSVCJJ model in case 1 (N, E) holds the same number of parameters with the HSVIJJ model in case 2 (Db-E, E) and in case 4 (E, Db-E), but the former (i.e. the HSVCJJ model) has the best market fit.

(2) We neither agree with a paradox, saying that the model specification has too many parameters to justify any conclusions. For this paradox followers, they may argue that the above market fit rankings can be explained in numerous other ways, in addition to the impact of distribution type of jump amplitude. However, we believe that a scientific analysis and comparison can always help to unearth the inner reasons for above fit rankings.

(3) We suggest that, it is impossible to understand the fit sequence without taking into account the properties of Db-E distribution, such as the leptokurtic feature and intrinsic asymmetry. Firstly, the leptokurtic feature of Db-E distribution itself is directly inherited by the return distribution (see Section 2.3 for details). Secondly, the data in Table 2 show, all db-E jumps in the calibrated HSVJJ models, no matter where they appear, in return or in variance, are asymmetric on this particular day, with uneven probabilities (i.e. $p \neq 0.5$) and different means (i.e. $\eta_u \neq \eta_d$) of upward and downward jumps, and distinct correlations (i.e. $\rho_u > \rho_d$) among simultaneous jumps. It is these good properties of Db-E distribution that drive the HSVJJ models to come out more skewed and leptokurtic distribution for return, thus leading to an improvement of fit to option markets. A similar argument can also be found in [28] where they reported the db-E jump-diffusion model performs better than the normal jump-diffusion model in fitting the indexes data, from an econometric perspective.

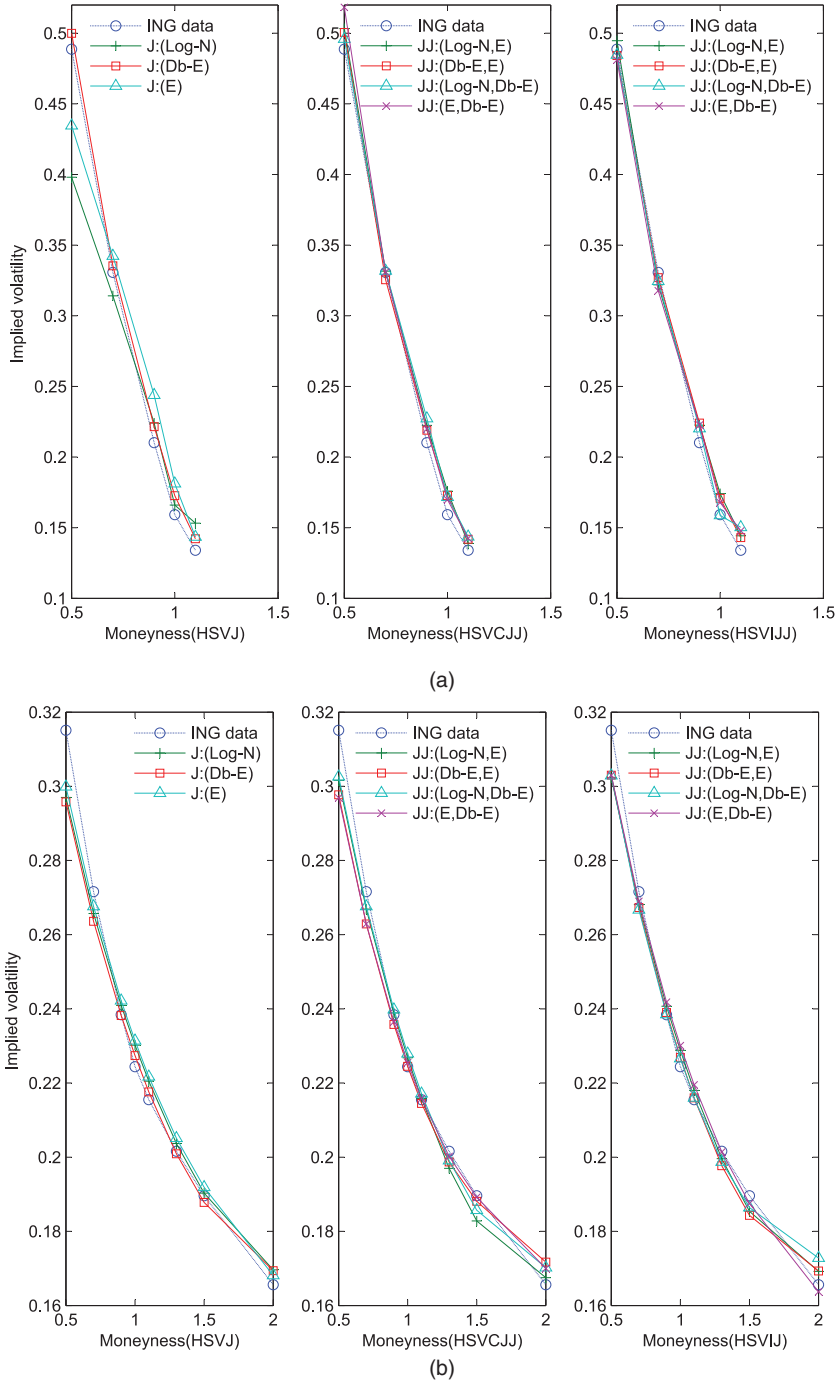

Figure 4. Volatility surfaces implied by ING Calls option with 1 month and 4 years to expiration. In figure, HSVJ is the Heston stochastic volatility model with jumps in return, HSVIJJ the Heston stochastic volatility model with independent jumps in return and variance, and HSVCJJ the Heston stochastic volatility model with simultaneous and correlated jumps in return and in variance. Notation J:(N) means the normal jump distribution, JJ:(N,E) means the combinatorial distributions of double jumps. The rest can be similarly understood. Model parameters are calibrated to the ING Calls options on 12 January 2005. (a) $T = 1$ m, (b) $T = 4y$.

Tables 2 and 3 also reveal some interesting parametrization patterns to the HSVJJ models. By adding a jump in volatility to the HSVJ model, generally we see a decline in the level of parameter ξ for all HSVIJJ models. This pattern has also been observed by Duffie *et al.* [8]. Besides, we see a significant decline in the level of parameter κ, and such a decline trend in κ continues with inclusion of instantaneous correlations among double jumps. Though Table 3 witnesses a few weak abnormities of 'κ'- and 'ξ'-pattern in ten independent runs, we attribute these abnormities to the local optima of high-dimensional numerical optimization. These interesting patterns suggest that all recalibrated parameters in four cases of HSVCJJ models, are both meaningful and stable, thanks to their good analytical tractability for options.

To show graphically how the type of jump amplitude distribution affects the market fit of stochastic volatility models, we plot the volatility surfaces of a very short (to say, 1 month) and a much long (4 years) expiration options under the HSVJ, HSVIJJ and HSVCJJ models, in Figure 4.

For both maturities, we find on this particular day the HSVJ, HSVIJJ and HSVCJJ models with the Db-E jumps, no matter they locate in return or in variance, have relatively better overall fits than the models with jumps governed by other distributions. Interestingly, the normally distributed jump amplitude that ever-prevailingly assumed in the canonical literature, performs not very well in capturing the implied volatility smirks.

4.2. Dynamic impacts on implied volatility of the transition of jump amplitude distribution type

This section, going beyond the static fitting exercise, investigates how the shift of jump amplitude distribution from the normal (and single exponential) distribution to the asymmetric db-E distribution might affect the implied volatility surfaces.

For this task, we carefully design three groups of experiments (see Table 4 for details):

- *Experiment #1: (N,E)→(Db-E,E).* For the fitted HSVIJJ model in Case 1 $(R-J, V-J) = (N, E)$, we tune parameters μ_J and σ_J in the normal distribution one by one, while fixing the remainings, and then observe the induced changes on the implied volatility surfaces. Similarly, for the HSVIJJ model in Case 2 $(R-J, V-J) = (Db-E, E)$, we tune parameters η_u and η_d in the db-E distribution, and observe the resulted the changes on the implied volatility surfaces. By comparing both changes, we access the difference of impacts on the implied volatilities driven by the transition of return-jump amplitude distribution from 'N' to 'Db-E'.

Table 4. Experiment arrangements for studying the dynamic impacts on the implied volatility surface of the transition of type of jump amplitude distribution.

Exp#	Fix: the remainings of HSVIJJ model[a]	Vary[b]:	Note
		$\mu_J \in \{0.01, 0.1, 0.2, 0.3, 0.4\}$	
	Case1: (R-J,V-J) = (N,E)	$\sigma_J \in \{0.01, 0.1, 0.2, 0.3, 0.4\}$	(*N*,E)
1		$\eta_u \in \{0.01, 0.1, 0.2, 0.3, 0.4\}$	→
	Case 2: (R-J,V-J) = (Db-E,E)	$\eta_d \in \{0.01, 0.1, 0.5, 1, 2\}$	(*Db-E*,E)
	Case 1: (R-J,V-J) = (N,E)	$\eta_J \in \{0.01, 0.1, 0.2, 0.3, 0.4\}$	(N,*E*)
2		$\eta_u \in \{0.01, 0.1, 0.2, 0.3, 0.4\}$	→
	Case 3: (R-J,V-J) = (N,Db-E)	$\eta_d \in \{0.01, 0.1, 0.5, 1, 2\}$	(N,*Db-E*)
		$\lambda_v = 0.1113$;	
	Case 3: (R-J,V-J) = (N,Db-E)	$p \in \{0, 0.25, 0.5, 0.75, 1\}$	Additional test
3		$\eta_u = 0.4557$; $\eta_d = 1.0721$;	of the goodness
	Case 2: (R-J,V-J) = (Db-E,E)	$p \in \{0, 0.25, 0.5, 0.75, 1\}$	of Db-E

[a] We use the HSVIJJ model rather than the HSVCJJ model, due to Ockham's Razor. Besides, the reason for hiring the fitted models rather than randomly parametrized models is: the fitted models to the same option data have a common ground for fair comparisons.

[b] All variations of parameters are assigned such that the hard constrains attached to the existence of the moment-generating functions are satisfied.

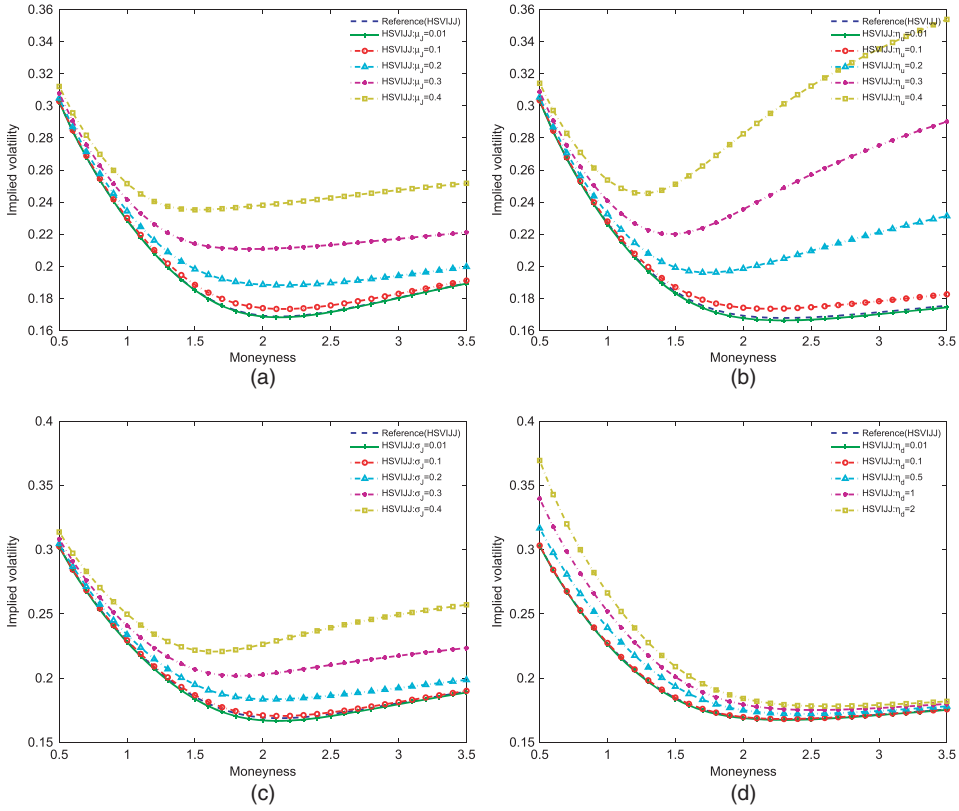

Figure 5. Four-year smile curve, replacing the return-jump distribution from the normal distribution to the asymmetric db-E distribution, i.e. (**N**,E)→(**Db-E**,E). HSVIJJ is the Heston volatility model with jumps in return and in variance, but without instantaneous correlation. (a) HSVIJJ in Case 1: varying μ_J, (b) HSVIJJ in Case 2: varying η_u, (c) HSVIJJ in Case 1: varying σ_J, and (d) HSVIJJ in Case 2: varying η_d.

- *Experiment #2: (N,E)→(N,Db-E).* For the fitted HSVIJJ model in Case 1 $(R-J, V-J) = (N, E)$ and in Case 3 $(R-J, V-J) = (N, Db-E)$, we follow the procedures described in Experiment #1. By this, we inspect the difference of impacts on the implied volatilities driven by the shift of variance jump amplitude distribution from 'E' to 'Db-E'.
- *Experiment #3:* For further demonstrating the performance of HSVJJ model with Db-E jump in capturing the option market, we inspect the impact on the implied volatility of parameter p, by varying it from 0 to 1 equidistantly with interval 0.25. Since the Db-E jump amplitude can be both the size of return jump and of variance jump, we take the fitted HSVIJJ model of Case 2 and Case 3 as two independent references. Moreover, to clearly display the impact of p on the implied volatilities, we cautiously take a large value for η_u and η_d in Case 2, for example, $\eta_u = 0.4557$ and $\eta_d = 1.0721$; and $\lambda_v = 0.1113$ in Case3. Here, 'cautiously' means all parameters taken here are such that the correspondent moment-generating functions are well defined.

The implied four-year volatility surfaces for the above variations are plotted in Figure 5–7, respectively. Due to the limit of length, we do not provide the experiments results for other maturities.

Figure 5 displays, with the replacement of the combinatorial distributions from (N,E) to (Db-E,E), the impacts on implied volatilities caused by varying parameters μ_J and σ_J in the normal distribution are quite different from those driven by tuning η_u and η_d in the db-E distribution. Figure 5(a) and 5(c) shows, enlarging μ_J and σ_J increases evidently the level and the curvature of implied volatility

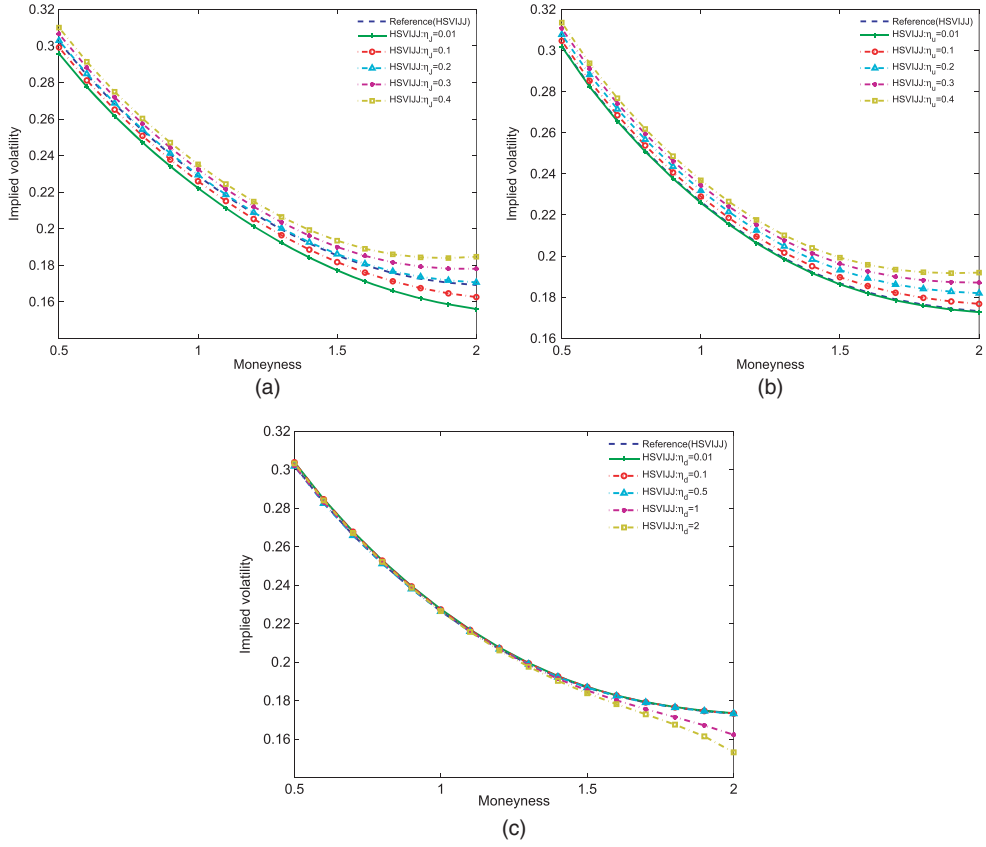

Figure 6. Four-year smile curve, replacing the variance jump distribution from the single-exponential distribution to the db-E distribution, i.e. (N,**E**)→(N,**Db-E**). (a) HSVIJJ in Case 1: varying η_J, (b) HSVIJJ in Case3: varying η_u, and (c) HSVIJJ in Case 3: varying η_d.

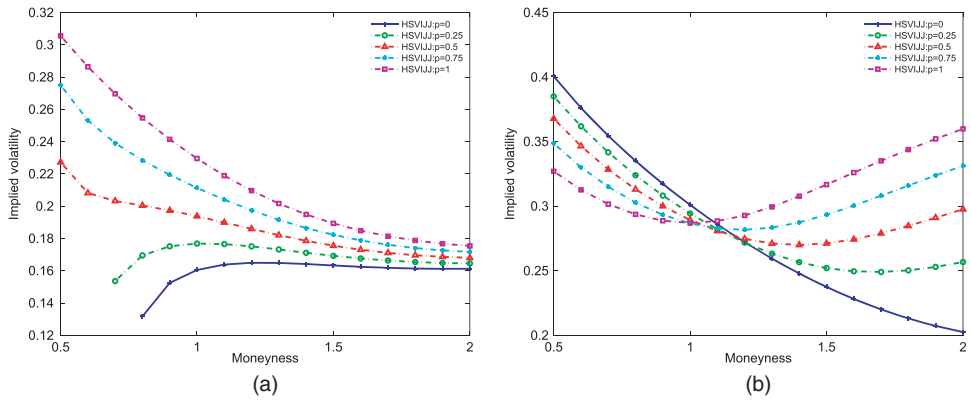

Figure 7. Four-year smile curve, varying the probability p of upward and downward jumps in the db-E distribution. (a) Jumps in variance $\sim$(Db-E): Fixing the fitted HSVIJJ of Case 3 with $\lambda_v = 0.1113$, (b) Jumps in variance $\sim$(Db-E): Fixing the fitted HSVIJJ of Case 2 with $\eta_u = 0.4557$, $\eta_d = 1.0721$.

surfaces; while Figure 5(b) and 5(d) displays, increasing parameters η_u and η_d, not only uplifts both the level and curvature, but also steepens the slope of option smirks.

Figure 6(a) and 6(b) presents, with the transition of the combinatorial distributions from (N,E) to (N,Db-E), tuning the upward-jump parameter η_J in the single-exponential function and η_u in the

db-E function, yields similar impacts on the implied volatility surfaces. It is easy to understand this. Figure 6(c) displays, increasing parameter η_d in the db-E jump, lowers the level of volatilities, with magnitudes depending on parameter p and λ_v. Since $p = 0.9479$ in the fitted HSVIJJ model of Case 3, meaning that almost no downward jumps would happen to the variance process, thus any changes in η_d may make little difference to the implied volatility, just as displayed in Figure 6(c).

Figure 7 reveals that the controlling probability p of upward jumps in the db-E distribution, uniting with parameters η_u, η_d and λ_v (or λ_s), has very profound impacts on the implied volatility surface. Figure 7(a) shows that, if the amplitude of variance jump is governed by the Db-E distribution, an increasing probability p, generally uplifts the values of OTM Puts. This is intuitive: when p increases, meaning an increasing probability of positive jumps will happen to the variance process, this further implies the market will fluctuate fiercely with a large probability due to the rise in implied volatility,

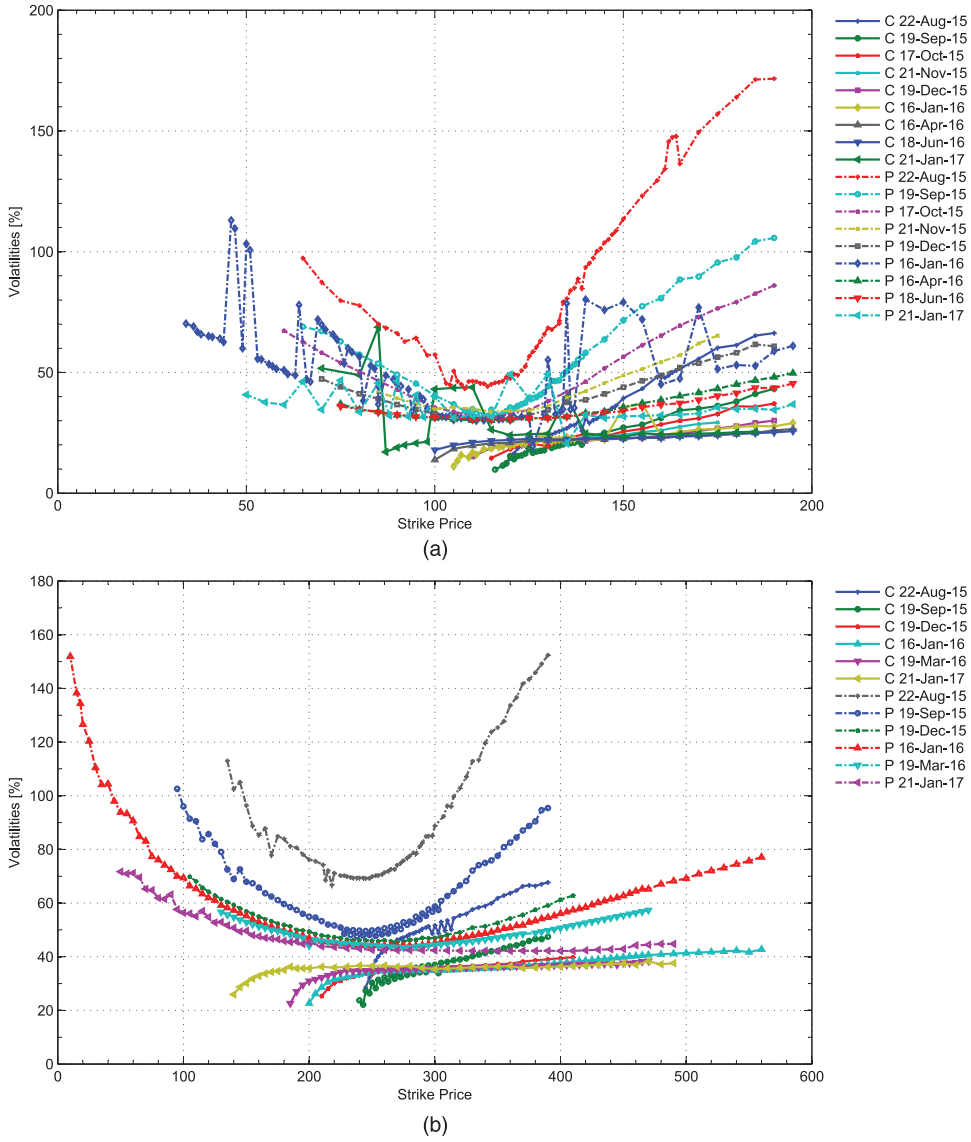

Figure 8. Volatility surfaces implied by two groups of American-style options, traded in NASDAQ on 4 August 2015. The figure here is output directly by the *OptionsOracle* tool. (a) Apple Inc. and (b) Tesla Motors, Inc.

thus the ITM call/OTM put value should be remedied positively. Conversely, a decreasing p means an increasing probability of negative jumps will happen to the variance, which implies the market is becoming smooth, therefore a negative correction should be made to the Black–Scholes model-based ITM call/OTM put value.

Interestingly, this thus results in a rising volatility surface as the strike increases (see the bottom curve in Figure 7(a)). We call this pattern of volatility curve 'sadness', mainly as response to the volatility 'smile' and 'smirk'. Though this new 'face' has been seldom reported before, we can observe it easily from real option markets. For example, the AAPL options written on stock Apple Inc. and the TSLA options written on Tesla Motors, Inc. (both traded in NASDAQ) implied volatility surfaces (on 4 August 2015) have evidently shown such a sad face, in addition to the smile and smirk, see Figure 8.

However, it is quite a different sightseeing for the HSVIJJ model with jump amplitude in return governed by the db-E distribution. Figure 7(b) shows that, an increasing p, generally decreases the values of OTM Puts, but uplifts the values of OTM Calls. This also can be easily understood: when p increases, meaning an increasing probability of positive jumps will happen to the price process, in other words, the market is taking off, hence the OTM call value increases.

Figure 7 indicates that, the HSVJJ model with double-exponentially distributed jump amplitudes can capture a variety of option markets, not matter the underlying market is expected to fluctuate turbulently or move smoothly.

5. Concluding remarks

Based on the explicit formula of European plain options under the HSVJJ model, this research concludes after extensive model calibrations and carefully designed implied-volatility impacting experiments that, the Db-E jump-size distribution, thanks to its leptokurtic feature and intrinsic asymmetry, but the scale of parameters contained, contributes the most significantly to improving the HSVJJ model's market fit to option data, among all three (i.e. N, E and Db-E) distributions, no matter the jumps locate in return or in variance. The Db-E jump-size distribution helps the HSVJJ model to capture a variety of financial markets, from very turbulent to calm; more interestingly, with this distribution, we observe not only the implied volatility smile and smirk, but also the volatility sadness.

This research suggests that the distribution type of jump amplitude does matter for the performances of jump-diffusion models, and the Db-E jump-size distribution seems to have both superiority and universality in describing the financial markets.

Notes

1. One can easily extend the 'constant' intensity to the stochastic case. For details, please see, e.g. [20]
2. For details, please visit https://en.wikipedia.org/wiki/Feynman-Kac_formula.
3. First, the second equation in PDEs formula (10) is a standard Riccati equation whose explicit solution has already been known. After having obtained $Q(\tau, \Omega)$, one can easily get $P(\tau, \Omega; J_s, J_v)$ by simple integral operation. Actually, Heston [19] and Duffie *et al.* [8] among others, have presented a detailed description about the derivation process.
4. To be rigorous, the return-jump distribution function $\varpi(J_s|J_v)$ should be written as below:

$$\varpi(J_s|J_v) = p\frac{1}{\eta_u}\mathrm{e}^{-1/\eta_u(J_s-\rho_u J_v)}\mathbf{1}_{J_s\geq\rho_u J_v} + q\frac{1}{\eta_d}\mathrm{e}^{1/\eta_d(J_s-\rho_d J_v)}\mathbf{1}_{J_s\leq\rho_d J_v}$$
$$+(1-p-q)\begin{cases}0, & \text{if } \rho_u=\rho_d;\\ \dfrac{1}{(\rho_u-\rho_d)J_v}\mathbf{1}_{\rho_d J_v<J_s<\rho_u J_v}, & \text{otherwise;}\end{cases}$$

   where $0<\eta_u<1, \eta_d>0; p, q\geq 0; \rho_u\geq\rho_d, \rho_u\eta_J<1$ and $\rho_d\eta_J<1$.In this work, since we are only interested in the impacts of the regular form of db-E function on market fit, the piecewise function $\varpi(J_s|J_v)$ on the domain $\rho_d J_v<J_s<\rho_u J_v$, is deliberately omitted, by simply taking $p+q=1$.
5. Please note that, all cumulants $c_1, c_2, c_4, \ldots$, are obtained via the connection between cumulant and the moment-generating function (which has been provided in Section 3.2). For details, please visit

https://en.wikipedia.org/wiki/Cumulant, where a very complicated technical document about how to derive 'cumulant' from the moment-generating function is provided.

6. The implementation code is programmed with Matlab language and executed on a PC equipped with Win7(64bit) and Intel(R) Xeon(R) CPU E5-1620 v2 @3.70GHz 3.70GHz RAM 8.00GB.
7. This work uses the standard solver *lsqnonlin* in Matlab to solve the optimization problem. In this solver, the Levenberg–Marquardt algorithm (LMA) is chosen, thanks for its excellent performance in solving the nonlinear least-squares problems. We notice that the LMA finds only a local minimum. Hence, we repeat calibrations independently for 10 times, with randomized initial start for each time.

Acknowledgments

For helpful comments and suggestions, we thank two anonymous referees, Cornelis W. Oosterlee, Jari Toivanen, Vladimir Kozlov, and seminar participants at the 2nd and 3rd Finance and Computing Forum, Finance and Management Science section of the 8th International Congress on Industrial and Applied Mathematics, the 12th and 13th International Symposium on Financial System Engineering and Risk Management.

Disclosure

No potential conflict of interest was reported by the authors.

Funding

This work was supported by the Natural Science Foundation of Guangdong Province, China under Grant [No. 2014A030313514].

ORCID

Y. Sun http://orcid.org/0000-0002-8984-5733

References

[1] Y. Achdou, G. Indragoby, and O. Pironneau, *Volatility calibration with American options*, Methods Appl. Anal. 11 (2004), pp. 533–556.
[2] L. Andersen, *Simple and efficient simulation of the Heston stochastic volatility model*, J. Comput. Financ. 11 (2008), pp. 1–42.
[3] D.S. Bates, *Jump, stochastic volatility: Exchange rate processes implicit in Deutsche Mark in options*, Rev. Financ. Stud. 9 (1996), pp. 69–107.
[4] P. Bjerksund and G. Stensland, *Closed-form approximation of American options*, Scand. J. Manag. 9(Suppl.) (1993), pp. S88–S99.
[5] P. Bjerksund and G. Stensland, *Closed form valuation of American options*, Discussion paper 2002. Available at http://citeseerx.ist.psu.edu/viewdoc/summary?doi = 10.1.1.202.5098.
[6] M. Broadie and O. Kaya, *Exact simulation of stochastic volatility and other affine jump diffusion processes*, Oper. Res. 54 (2006), pp. 217–231.
[7] L. Chen, *Stochastic mean and stochastic volatility a three-factor model of the term structure of interest rates and Its application to the pricing of interest rate derivatives*, Financ. Markets, Inst, Instrum. 5 (1996), pp. 1–88.
[8] D. Duffie, J. Pan, and K. Singleton, *Transform analysis and asset pricing for affine jump-diffusions*, Econometrica 68 (2000), pp. 1343–1376.
[9] F. D'Ippoliti, E. Moretto, S. Pasquali, and B. Trivellato, *Exact pricing with stochastic volatility and jumps*, Int. J. Theor. Appl. Financ. 13 (2010), pp. 901–929.
[10] B. Eraker, M. Johannes, and N. Polson, *The impact of jumps in volatility and returns*, J. Financ. 58 (2003), pp. 1269–1300.
[11] F. Fang and C.W. Oosterlee, *A novel pricing method for European based on Fourier-cosine series expansions*, SIAM J. Sci. Comput. 31 (2008), pp. 826–848.
[12] F. Fang, *The COS method: An efficient Fourier method for pricing financial derivatives*, Ph.D. thesis in Math. Numer. Anal. Group, Delft Univ. Tech., 8 December 2010.
[13] F. Fang and C.W. Oosterlee, *A Fourier-based valuation method for Bermudan and barrier options under Heston's model*, SIAM J. Financ. Math. 2 (2011), pp. 439–463.
[14] K. Giesecke and D. Smelov, *Exact Sampling of Jump Diffusions*, Oper. Res. 61 (2013), pp. 894–907.
[15] L. Grzelak and C. Oosterlee, *An equity-interest rate hybrid model with stochastic volatility and the interest rate smile*, J. Comput. Financ. 15 (2012), pp. 45–77.

[16] L.A. Grzelak, C.W. Oosterlee, and S. van Weeren, *Extension of stochastic volatility models with Hull–White interest rate process*, Quant. Financ. 12 (2012), pp. 89–105.
[17] P. Hagan, D. Kumar, A. Lesniewski, and D. Woodward, *Managing smile risk*, Wilmott Mag. 7 (2002), pp. 84–108.
[18] F. Hanson, *Stochastic-volatility, jump-diffusion optimal portfolio problem with jumps in returns and volatility*, Working paper, June 18, 2011. Available at SSRN: http://ssrn.com/abstract = 1874872 or http://dx.doi.org/10.2139/ssrn.1874872.
[19] S.L. Heston, *A closed form solution for options with stochastic volatility with applications to bonds and currency options*, Rev. Financ. Stud. 6 (1993), pp. 327–343.
[20] J. Huang, W. Zhu, and X. Ruan, *Option pricing using the fast Fourier transform under the double exponential jump model with stochastic volatility and stochastic intensity*, J. Comput. Appl. Math. 263 (2014), pp. 152–159.
[21] K. Ignatieva, P. Rodrigues, and N. Seeger, *Stochastic volatility and jumps: Exponentially affine yes or no? An empirical analysis of S&P500 dynamics*, Goethe University Frankfurt, Working Paper, 2009.
[22] S.G. Kou, *A jump-diffusion model for option pricing*, Manag. Sci. 48 (2002), pp. 1086–1101.
[23] S. Kou, *Jump-diffusion models for asset pricing in financial engineering*, in *Handbooks in OR & MS*, Vol. 15, J.R. Birge and V. Linetsky, eds., Elsevier Science, Amsterdam, 2008, pp. 74–116.
[24] E. Lindström, J. Ströjby, M. Brodén, M. Wiktorsson, and J. Holst, *Sequential calibration of options*, Comput. Stat. Data Anal. 52 (2008), pp. 2877–2891.
[25] N. Makate and P. Sattayatham, *Stochastic volatility jump-diffusion model for option pricing*, J. Math. Financ. 1 (2011), pp. 90–97.
[26] R. Merton, *Option pricing when underlying stock returns are discontinuous*, J. Financ. Econ. 3 (1976), pp. 125–144.
[27] W. Poklewski-Koziell, *Stochastic volatility models: Calibration, pricing and hedging*, MS thesis in Adv. Math. Financ, Sch. Comput. Appl. Math., Univ. Wits., May 2012.
[28] C.A. Ramezani and Y. Zeng, *Maximum likelihood estimation of the double-exponential jump-diffusion process*, Ann. Financ. 3 (2007), pp. 487–507.
[29] Y. Sun, *Efficient pricing and hedging under the double Heston stochastic volatility jump-diffusion model*, Int. J. Comput. Math. 92 (2015), pp. 2551–2574.
[30] W. Xu, C. Wu, and H. Li, *Foreign equity option pricing under stochastic volatility model with double jumps*, Econ. Model. 28 (2011), pp. 1857–1863.
[31] X. Zang, J. Ni, J. Huang, and L. Wu, *Double-jump stochastic volatility model for VIX: Evidence from VVIX*, Working paper, 1 July 2015. Available at http://arxiv.org/abs/1506.07554.
[32] B. Zhang and C. Oosterlee, *An efficient pricing algorithm for swing options based on Fourier cosine expansions*, J. Comput. Financ. 16 (2013), pp. 1–32.
[33] B. Zhang and C.W. Oosterlee, *Efficient pricing of European-style Asian options under exponential Lévy processes based on Fourier cosine expansions*, SIAM J. Financ. Math. 4 (2013), pp. 399–426.
[34] Z. Zhu, *Option Pricing and Jump Diffusion Models*, Ph.D. thesis in Mathematics, Dept. Math., Stat. & Comput. Sci., Univ. Il. at Chicago, 17 October 2005.
[35] Z. Zhu and F. Hanson, *Optimal portfolio application with double uniform jump model*, in *Stochastic Processes, Optimization, and Control Theory: Applications in Financial Engineering, Queueing Networks, and Manufacturing Systems: A Volume in Honor of Suresh Sethi, International Series in Operations Research and Management Science*, H. Yan, G. Yin, Q. Zhang, eds., Springer-Verlag, New York, Vol. 94, 2006, pp. 331–358.